Laser-amplifier gain and noise

R. Loudon and M. Harris
Physics Department, Essex University, Colchester CO4 3SQ, United Kingdom

T. J. Shepherd and J. M. Vaughan
Defence Research Agency, Royal Signals and Radar Establishment, St. Andrews Road, Great Malvern, Worcestershire WR14 3PS, United Kingdom

(Received 4 January 1993)

A theoretical study is presented of the gain and the noise spectra of laser amplifiers at pumping rates both above and below the oscillation threshold. The theory is valid for both class-A and class-B laser systems, where the decay rate of the collective atomic dipole moment greatly exceeds the decay rates of the atomic population inversion and the laser cavity. The gain and the noise properties are shown to be strongly influenced by a four-wave mixing of the signal and image frequencies via a modulation of the population inversion. Particular attention is paid to the residual noise flux that persists in the laser output above threshold and to the typical characteristics of a second-order phase transition displayed by the gain in the threshold region. The results for the above-threshold laser amplifier are compared with experimental measurements of both gain and noise for the argon-ion (class-A) and CO_2 (class-B) lasers. The signal-to-noise ratios for both heterodyne and direct-detection measurements are evaluated, and the conditions are determined under which optical amplification can lead to an enhancement of sensitivity.

PACS number(s): 42.60.Lh, 42.60.Mi, 42.79.Qx

I. INTRODUCTION

The laser has been the subject of extensive research and development for more than 30 years. The physical principles of its operation and many of its basic properties were elucidated in the late 1950s and in the 1960s. Its reputation at that time of being a solution in search of a problem is now difficult to reconcile with the wealth of its applications, not only as a tool in many fields of research, but also as an important component in equipment used in surgery and more generally in commerce and industry, in the office and in the home. The device is widely regarded as well understood, and current fundamental research on lasers is mainly focused on the development of novel varieties and on the understanding of its more esoteric features.

It has recently been shown, however, that even the most basic properties of one of the most commonplace of lasers, the argon-ion (Ar^+) laser, can be further explored by means of some experiments that are quite simple in concept. Thus the gain profile of the laser, whose form provides an essential component of any model of the workings of the device, has been determined for the first time by measurements of the amplification of an injected signal [1]. Furthermore, the noise spectrum of the laser has been studied experimentally [2,3], and it shows dramatic noise-cancellation effects that were apparently overlooked in previous work. The purpose of the present paper is to provide more complete details of the measurements and to interpret their results in terms of a comprehensive theory of laser gain and noise.

Continuous-wave lasers fall into three main classes defined by the relative magnitudes of the relaxation rates associated with the coupled atom-cavity system. The decay rate of the collective atomic dipole moment (which determines the spectral linewidth of the lasing transition) is here denoted by $\gamma_\perp$, that of the atomic population inversion (equal to the inverse of the atomic lifetime) by $\gamma_\parallel$, and that of the empty laser cavity (determined by the cavity length and loss) by γ_c. The time scales of the equations of motion of the atomic dipole moment, atomic inversion, and optical field are governed, respectively, by these three decay rates. The Ar^+ laser belongs to class A, specified by the condition $\gamma_\perp \gg \gamma_\parallel \gg \gamma_c$. In this case the atomic variables respond to the value of the optical field essentially instantaneously, and adiabatic or quasistatic approximations can be made in the two atomic equations of motion. Thus only the equation for the optical field retains its differential form, and this is straightforwardly solved to the level of approximation needed in the present work. The well-known Scully-Lamb model [4,5] is valid for class-A lasers. The simplicity of both theoretical and experimental results for class A greatly facilitates the understanding of basic laser physics.

Although most of our work is concerned with the Ar^+ laser, we have also made some measurements on the CO_2 laser, which belongs to class B, specified by the condition $\gamma_\perp \gg \gamma_\parallel \approx \gamma_c$. In this case only the equation of motion for the atomic dipole moment can be solved in an adiabatic approximation, leaving simultaneous differential equations for the atomic inversion and the optical field. These can again be solved to the required level of approximation without too much difficulty. The results are now more complicated than those for the class-A laser, to which they reduce when the further assumption $\gamma_\parallel \gg \gamma_c$ is made. Semiconductor lasers also belong to class B, although their behavior shows additional complexity on account of the significant coupling of phase and intensity

 ©1993 The American Physical Society

fluctuations [6]. Nevertheless, our results for the class-*B* noise spectrum, derived with the CO_2 laser in mind, can be compared with expressions derived for semiconductor lasers [7].

The final category of laser, class *C*, has three decay rates of comparable magnitude, $\gamma_\perp \approx \gamma_\parallel \approx \gamma_c$, and all three of the equations of motion must be retained in differential form. The existence of three active degrees of freedom is a requirement for the onset of chaotic behavior in laser systems [8], and class-*C* lasers have been much studied for the instabilities and chaos that occur for suitable ranges of the parameters. Class-*C* lasers are excluded from the analysis and experiments reported here.

The main body of the paper begins in Sec. II with a description of the laser model. In addition to the restriction to classes *A* and *B*, the laser is also assumed to have a "good" cavity, whose modes are sufficiently well separated in frequency for the experiments to excite only a single internal mode. The laser generally emits light into free space from both ends of the cavity, and we use the now well-established technique for matching a discrete internal-mode field to the continuous-mode external fields [7,9]. Both the Ar^+ ion and the CO_2 molecule move sufficiently rapidly to inhibit any spatial hole burning on the scale of the laser wavelengths. The lasing media are accordingly assumed to be homogeneous. The laser variables are treated as classical quantities, and the effects of the quantum noise sources are represented by Langevin forces. The laser dynamics are therefore described by the usual Maxwell-Bloch equations [5,10,11]. The equation of motion for the optical field is augmented for calculations of the gain by the driving force from an injected signal. The equation for the atomic dipole moment can be solved immediately with the exclusion from consideration of class-*C* lasers. The steady-state properties of the free-running laser are briefly derived in Sec. III.

The main calculations of the paper are presented in Secs. IV and V for the below-threshold and above-threshold lasers, respectively. The associated experimental results for gain and noise, obtained above threshold, are presented in Sec. VI. The gain determined by the amplification of an injected signal is considered in Secs. IV A and V A. Studies of the laser with an injected signal have a lengthy history, and it is necessary to place our contribution in the context of earlier research. We assume, and verify experimentally, that our injected signal is sufficiently weak for only *linear* amplification to occur. The measurements can thus be modeled by a theory that determines the linear part of the relation between output and input signal amplitudes. The linear gain, equivalent to a linear susceptibility, was considered by DeGiorgio and Scully [12] in their analogy between the laser threshold region and a second-order phase transition. One of our aims here is to present a more detailed account of the changes in linear gain that occur at threshold. The above-threshold linear gain has been considered previously by Pantell [13]. More generally, he and later authors [11,14–16] have treated the effects of stronger input signals that significantly modify the characteristics of the free-running laser by injection locking. The calculations need to be taken to second order in the signal amplitude in order to model injection locking, and this effect is excluded by the first-order treatment given here. The injection of stronger input signals also produces interesting instabilities [16], which again are not included here.

A major conclusion of the present work is the importance for the gain mechanism above threshold of four-wave mixing between the optical field at the frequency of the input signal and a field at the image frequency on the other side of the laser line. The four-wave mixing is driven by the strong laser field in the cavity via modulation of the population inversion. This modulation is closely related to the phenomenon of population pulsations [5] in a two-mode laser. As a consequence of this nonlinear coupling, signal and image fields of comparable magnitude but of approximately opposite phase are excited to first order in the amplitude of the input signal. Such four-wave-mixing processes have been considered before [17], with applications to the production of nonclassical light [18] and to the dynamics of semiconductor lasers [19]. However, the important cancellation effects in the observed heterodyne gain, produced by the resulting anticorrelation between the signal and image contributions, seem not to have been recognized previously.

Expressions for the laser noise spectra below and above threshold are derived in Secs. IV B and V B. The calculations make heavy use of well-established methods and results [10,20]. However, we make an identification of the important role played by anticorrelations between the noise contributions at signal and image frequencies on opposite sides of the laser line. The resulting partial cancellation of the noise observed in heterodyne detection parallels the gain cancellation mentioned above. This similarity in behavior confirms the close relationship between gain and noise expected for a linear amplifier [21].

The aim of the work outlined above is a better understanding of the gain and noise processes that underlie the operation of ordinary gas lasers. However, the experimental arrangement used in our measurements of the laser gain closely resembles that of the self-aligning (so-called "autodyne") laser radar [22,23]. A further motivation of the work is the desire to understand such systems. The detuned input signal is now obtained from a Doppler-shifted return beam produced by scattering of the laser output beam by a moving object. The velocity of the object may then be inferred from the modulation of the laser intensity from the opposite end of the cavity, caused by the beating of the amplified return signal and its image with the free-running laser beam. Signal-to-noise ratios for the laser amplifier below and above threshold are derived in Secs. IV C and V C, respectively. The more important above-threshold results can be used to assess the potential advantages of laser amplification for the performance of autodyne lidar systems.

II. LASER-AMPLIFIER MODEL

Figure 1 shows a representation of the laser cavity, with two mirrors of intensity transmission coefficients T_1 and T_2 separated by a distance L. The intensity damping rates associated with the two mirrors are given by

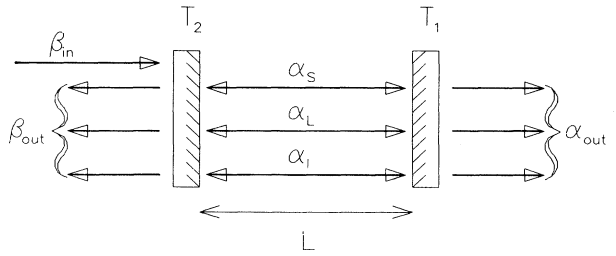

FIG. 1. Schematic arrangement of the amplifier cavity showing the notation for field amplitude components.

$$\gamma_1 = cT_1/2L \text{ and } \gamma_2 = cT_2/2L \ , \tag{2.1}$$

and the total damping rate of the internal field in the cavity is denoted

$$\gamma_c = \tfrac{1}{2}(\gamma_1+\gamma_2) \ . \tag{2.2}$$

The full width of the cavity mode intensity spectrum in angular frequency units (the empty-cavity bandwidth) is

$$\Gamma_0 = 2\gamma_c = \gamma_1+\gamma_2 \ . \tag{2.3}$$

In the presence of an inverted atomic population in the cavity, it is assumed that laser action occurs for a single mode of frequency ω_L in resonance with the atomic transition.

We seek the amplification characteristics of the laser for an input signal of complex amplitude β_{in} whose frequency is detuned from the laser frequency ω_L by a variable amount ω. Such an input excites a field α in the cavity, and for a cavity with highly reflecting mirrors, the output fields have complex amplitudes given by [9]

$$\alpha_{\text{out}} = \gamma_1^{1/2}\alpha \tag{2.4}$$

and

$$\beta_{\text{out}} = \gamma_2^{1/2}\alpha - \beta_{\text{in}} \ . \tag{2.5}$$

The relations between these two output fields and the input field β_{in} determine the amplifier gains in transmission and reflection, respectively.

The laser-amplifier dynamics are described by the usual Maxwell-Bloch equations [24]. The first of these is the equation of motion for the cavity field α in the form

$$\dot{\alpha}+(\gamma_c+i\omega_L)\alpha = gd+\gamma_2^{1/2}\beta_{\text{in}}+\Gamma_\alpha \ , \tag{2.6}$$

where the terms that occur on the right-hand side represent the forces that drive the field. These result, respectively, from the interaction of the collective atomic dipole moment d and the cavity field with coupling constant g, the input signal β_{in} that enters the cavity through the mirror whose transmission is described by γ_2, and a random Langevin force Γ_α that represents the effect on the cavity field of quantum noise sources. The equation of motion for the atomic population inversion D is

$$\dot{D}+\gamma_\parallel D = \gamma_\parallel D_p - g(\alpha^* d+\alpha d^*)+\Gamma_D \ , \tag{2.7}$$

where $\gamma_\parallel$ is the population-inversion decay rate. The terms on the right-hand side represent, respectively, the laser pump expressed in terms of the mean population inversion D_p that would be obtained in the absence of any cavity field, the driving force from the coupling of field and dipole moment, and a quantum-noise-induced Langevin force Γ_D for the population inversion. The equation of motion for the population inversion takes the simple form (2.7) only for laser transitions in which the lower-level population is negligible, and many of the results that follow are valid only when this perfect-inversion assumption is satisfied. The effects of significant lower-level population are discussed in the Appendix. The third and final Maxwell-Bloch equation is the equation of motion for the atomic dipole moment d in the form

$$\dot{d}+(\gamma_\perp+i\omega_L)d = g\alpha D+\Gamma_d \ , \tag{2.8}$$

where $\gamma_\perp$ is the dipole-moment decay rate. The forces on the right-hand side represent, respectively, the effects of coupling between the atomic population inversion and the cavity field, and the quantum-noise Langevin force for the dipole moment. Note that the variables α, D, and d, the input signal β_{in}, and the Langevin forces Γ are all functions of the time, but for reasons of simplicity this is not shown explicitly in the equations of motion.

Calculations of the laser gain and noise are presented in later sections of the paper. For linear amplification, it is necessary to obtain solutions of the equations of motion for the mean-field amplitudes correct to first order in β_{in}. The random forces have zero-mean values,

$$\langle\Gamma_\alpha\rangle = \langle\Gamma_D\rangle = \langle\Gamma_d\rangle = 0 \ , \tag{2.9}$$

and hence the Maxwell-Bloch equations can be simplified by removal of the Langevin forces for the gain calculation. It is convenient to express the input signal field in the form

$$\beta_{\text{in}} = \beta_S \exp[-i(\omega_L+\omega)t] \ , \tag{2.10}$$

where the detuning ω can be positive or negative. It will be shown that to first order in β_S, there are contributions to the internal field α at frequencies $\omega_L+\omega$ (signal) and $\omega_L-\omega$ (image) in addition to the zero-order free-running laser field at frequency ω_L. The average internal field thus has the form

$$\alpha = \alpha_L \exp(-i\omega_L t)+\alpha_S \exp[-i(\omega_L+\omega)t] + \alpha_I \exp[-i(\omega_L-\omega)t] \ . \tag{2.11}$$

The mean collective atomic dipole moment has the similar form

$$d = d_L \exp(-i\omega_L t)+d_S \exp[-i(\omega_L+\omega)t] + d_I \exp[-i(\omega_L-\omega)t] \ . \tag{2.12}$$

There are also three terms in the mean population inversion

$$D = D_0+D_1 \exp(-i\omega t)+D_1^* \exp(i\omega t) \ , \tag{2.13}$$

where D_0 is the constant population inversion of the

free-running laser and D_1 is of first order in the input signal amplitude. The occurrence of both signal and image field amplitudes, α_S and α_I, to first order in β_S is a signature of the nondegenerate four-wave-mixing process that controls the amplification. These amplitudes are coupled by the D_1 modulation ("population pulsation" [5]) terms in the population inversion (2.13).

For calculations of the noise, it is necessary to consider the fluctuations of the field variables around their mean values. The noise spectra are determined by averages of products of pairs of the Langevin forces, and the Γ must now be retained in the Maxwell-Bloch equations. The input field β_{in} can, however, be removed from (2.6) in calculations of the basic laser noise. In addition, for temperatures sufficiently low that there is no significant thermal excitation at frequency ω_L, we may put

$$\Gamma_\alpha = 0 , \tag{2.14}$$

since any contributions from this force are negligibly small [10].

If class-C lasers are excluded from consideration, $\gamma_\perp$ can be assumed much larger than the detuning ω and the cavity decay rate γ_c, and the resultant homogeneous broadening thus dominates the inhomogeneous Doppler broadening. Under this condition, spectral hole burning effects may be assumed to be negligible. Then (2.8) is well approximated by

$$\gamma_\perp d = g\alpha D + \Gamma_d . \tag{2.15}$$

Thus d can be eliminated from (2.6) and (2.7), leaving only two equations of motion for solution.

III. FREE-RUNNING LASER

When there is no input signal, $\beta_{\text{in}}=0$, and the Langevin forces are neglected, the quantities α_S, α_I, d_S, d_I, and D_1 in the solutions (2.11), (2.12), and (2.13) all vanish, and the Maxwell-Bloch equations (2.6), (2.7), and (2.15) reduce to

$$\gamma_c \alpha_L = g d_L , \tag{3.1}$$

$$\gamma_\parallel D_0 = \gamma_\parallel D_p - g(\alpha_L^* d_L + \alpha_L d_L^*) , \tag{3.2}$$

$$\gamma_\perp d_L = g \alpha_L D_0 . \tag{3.3}$$

These equations determine the mean values of the laser variables.

There are two forms of solution, one of which is

$$\alpha_L = 0 , \quad d_L = 0 , \quad D_0 = D_p . \tag{3.4}$$

This corresponds to the laser below threshold, with a zero mean-field amplitude and a population inversion proportional to the pumping rate. It can be shown that (3.4) is the stable solution when the cooperation parameter or normalized pumping rate defined by

$$C = g^2 D_p / \gamma_c \gamma_\perp \tag{3.5}$$

has a value smaller than unity, $C < 1$.

The other form of solution corresponds to the laser above threshold, and it is stable for $C > 1$. It has a field amplitude given by

$$|\alpha_L|^2 = (D_p - D_0)\gamma_\parallel / 2\gamma_c , \tag{3.6}$$

where the population inversion

$$D_0 = \gamma_c \gamma_\perp / g^2 \tag{3.7}$$

is independent of the laser pumping rate. The internal field intensity or mean photon number (3.6) can be written in the compact form

$$|\alpha_L|^2 = (C-1) n_S , \tag{3.8}$$

where

$$n_S = \gamma_\perp \gamma_\parallel / 2g^2 \tag{3.9}$$

is called the saturation photon number; that is, the number of photons stored in the laser cavity at twice-threshold pumping rate. Correspondingly, the laser output at this pumping rate is called the saturation power P_S. The laser power from the α_{out} end may conveniently be expressed as

$$P = P_S (C-1) , \tag{3.10}$$

with P_S given by

$$P_S = \hbar \omega_L \gamma_1 n_S . \tag{3.11}$$

IV. BELOW-THRESHOLD LASER AMPLIFIER

The theory of an inverted-population cavity amplifier operated below its laser threshold has been extensively treated by Mander, Loudon, and Shepherd [25] (this paper and its equations are identified by the abbreviation MLS). The treatment of MLS was based on quantum Langevin equations and the results were expressed in terms of relations between the input and output field operators of the amplifier. The theory presented here uses c-number field variables and the model of the amplifier is somewhat more versatile than that of MLS, although it is valid only for classical fields. The main properties of the below-threshold laser amplifier are rederived in the present section for the purposes of completeness and comparison with the above-threshold results given in the following section.

A. Gain

The laser variables below threshold are given by (3.4). In addition, in the absence of any strong coherent laser line with frequency ω_L, there is no mean excitation of the image-frequency field and no modulation of the population inversion, so that

$$\alpha_I = 0 , \quad d_I = 0 , \quad D_1 = 0 . \tag{4.1}$$

Thus, only the signal-frequency contribution survives in the internal field (2.11) and the collective dipole moment (2.12). The mean internal signal-field amplitude is thus determined by the Maxwell-Bloch equations (2.6) and (2.15), which reduce to

$$(\gamma_c - i\omega)\alpha_S = g d_S + \gamma_2^{1/2} \beta_S \tag{4.2}$$

and

$$\gamma_\perp d_S = g\alpha_S D_p \ . \tag{4.3}$$

The solution is

$$\alpha_S = \frac{\gamma_2^{1/2}\beta_S}{\gamma_c(1-C)-i\omega} \ , \tag{4.4}$$

where the cooperation parameter C defined in (3.5) is smaller than unity.

We define the below-threshold complex amplitude gain in transmission by

$$g_T = \frac{\alpha_{\text{out}}}{\beta_S} = \frac{(\gamma_1\gamma_2)^{1/2}}{\gamma_c(1-C)-i\omega} \ , \tag{4.5}$$

where (2.4) has been used, and the corresponding intensity transmission gain is

$$G_T(\omega) = |g_T|^2 = \frac{\gamma_1\gamma_2}{\omega^2+\gamma_c^2(1-C)^2} \ . \tag{4.6}$$

The peak gain is accordingly

$$G_T(0) = \gamma_1\gamma_2/\gamma_c^2(1-C)^2 \tag{4.7}$$

and this is greater than unity for

$$C > (\gamma_1^{1/2}-\gamma_2^{1/2})^2/(\gamma_1+\gamma_2) \ . \tag{4.8}$$

The lower part of the shaded region in Fig. 2 shows the ranges of values of C and γ_1/γ_2 for which the peak gain exceeds unity. The full width of the gain profile at half-maximum height is

$$\Gamma = 2\gamma_c(1-C) = \Gamma_0(1-C) \ , \tag{4.9}$$

where the empty-cavity bandwidth Γ_0 is defined in (2.3). It is seen that the peak gain increases while the gain bandwidth diminishes as the normalized pumping rate C is increased towards its threshold value of unity. From (4.7) and (4.9) it is easily shown that the product of the bandwidth and the square root of the peak gain is a constant. Similar results for the bandwidth and the gain profile were found in MLS(2.13) and MLS(3.5).

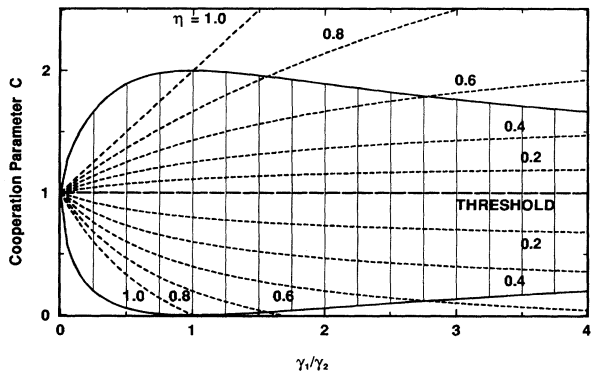

FIG. 2. The shaded area shows the values of cooperation parameter C and cavity-mirror decay rates for which the amplifier gain exceeds unity for zero detuning. The dashed curves show the parameter values that maximize the heterodyne signal-to-noise ratio for different values of the detection efficiency η.

The below-threshold gains in reflection are defined analogously by

$$g_R = \frac{\beta_{\text{out}}}{\beta_S} = \frac{\gamma_2^{1/2}\alpha_S}{\beta_S} - 1 \ , \tag{4.10}$$

where (2.5) has been used, and

$$G_R(\omega) = |g_R|^2 = \frac{4\omega^2+[-\gamma_1+\gamma_2+(\gamma_1+\gamma_2)C]^2}{4\omega^2+(\gamma_1+\gamma_2)^2(1-C)^2} \ , \tag{4.11}$$

where (4.4) has been used. Note that

$$G_R(\omega) = 1 \quad \text{for } C = \gamma_1/(\gamma_1+\gamma_2) \ , \tag{4.12}$$

and the gain is greater than unity for larger values of C.

B. Noise

In order to calculate the laser-amplifier noise spectrum, we use the Maxwell-Bloch equations (2.6), (2.7), and (2.15) with the forces Γ_D and Γ_d retained but the signal input amplitude β_{in} set equal to zero. The mean laser field α_L continues to vanish, as in (3.4), but we look for zero-mean fluctuations in the field by setting

$$\alpha(t) = \delta\alpha(t)\exp(-i\omega_L t) \ , \tag{4.13}$$

where the time dependence of variables is now shown explicitly to distinguish them from their Fourier transforms. The population inversion is also assigned a fluctuating contribution,

$$D(t) = D_p + \delta D(t) \ . \tag{4.14}$$

These trial solutions are now substituted into the Maxwell-Bloch equations, and the terms of first order in the fluctuating variables and forces give

$$\delta\dot{\alpha}(t)+\gamma_c(1-C)\delta\alpha(t) = (g/\gamma_\perp)\Gamma_d(t)\exp(i\omega_L t) \tag{4.15}$$

and

$$\delta\dot{D}(t)+\gamma_\parallel\delta D(t) = \Gamma_D(t) \ , \tag{4.16}$$

where the definition (3.5) of the cooperation parameter C has been used again.

We define Fourier transforms of the time-dependent quantities according to

$$\delta\alpha(\omega) = (2\pi)^{-1/2}\int dt\, \exp(i\omega t)\delta\alpha(t) \ , \tag{4.17}$$

where in view of (4.13) ω is measured with respect to the laser frequency ω_L. The equations of motion (4.15) and (4.16) are readily solved to obtain

$$\delta\alpha(\omega) = \frac{(g/\gamma_\perp)\Gamma_d(\omega_L+\omega)}{-i\omega+\gamma_c(1-C)} \tag{4.18}$$

and

$$\delta D(\omega) = \frac{\Gamma_D(\omega)}{-i\omega+\gamma_\parallel} \ . \tag{4.19}$$

The power spectra of the fluctuations are then obtained by evaluation of the averages

$$\langle \delta\alpha^*(\omega)\delta\alpha(\omega')\rangle = \frac{(g/\gamma_\perp)^2\langle \Gamma_d^*(\omega_L+\omega)\Gamma_d(\omega_L+\omega')\rangle}{[i\omega+\gamma_c(1-C)][-i\omega'+\gamma_c(1-C)]} \tag{4.20}$$

and

$$\langle \delta D(\omega)\delta D(\omega')\rangle = \frac{\langle \Gamma_D(\omega)\Gamma_D(\omega')\rangle}{(-i\omega+\gamma_\parallel)(-i\omega'+\gamma_\parallel)} . \tag{4.21}$$

The Langevin force correlation functions that occur in these expressions can be obtained by straightforward adaptation of results given by Louisell [10], in the forms

$$\langle \Gamma_d^*(\omega_L+\omega)\Gamma_d(\omega_L+\omega')\rangle = 2\gamma_\perp D_p\delta(\omega-\omega') \tag{4.22}$$

and

$$\langle \Gamma_D(\omega)\Gamma_D(\omega')\rangle = 2\gamma_\parallel D_P\delta(\omega+\omega') , \tag{4.23}$$

where δ denotes the Dirac δ function. The required noise power spectra are therefore

$$\langle \delta\alpha^*(\omega)\delta\alpha(\omega')\rangle = \frac{2\gamma_c C}{\omega^2+\gamma_c^2(1-C)^2}\delta(\omega-\omega') \tag{4.24}$$

and

$$\langle \delta D(\omega)\delta D(\omega')\rangle = \frac{2\gamma_\perp D_p}{\omega^2+\gamma_\parallel^2}\delta(\omega+\omega') . \tag{4.25}$$

The time-dependent field correlation function obtained by Fourier transformation of (4.24) is

$$\langle \alpha^*(t)\alpha(t')\rangle = \frac{C}{1-C}\exp[i\omega_L(t-t') - \gamma_c(1-C)|t-t'|] . \tag{4.26}$$

This has the well-known form characteristic of purely chaotic light [26] with mean photon number

$$\langle n\rangle = C/(1-C) , \tag{4.27}$$

in agreement with the standard result for a laser below threshold [5,26]. In terms of this intracavity photon number, the bandwidth (4.9) can be written as

$$\Gamma = 2\gamma_c C/\langle n\rangle , \tag{4.28}$$

and the correlation function (4.26) is

$$\langle \alpha^*(t)\alpha(t')\rangle = \langle n\rangle\exp[i\omega_L(t-t') - C\gamma_c|t-t'|/\langle n\rangle] . \tag{4.29}$$

The above properties refer to the chaotic light inside the below-threshold laser cavity. With use of the relation (2.4) between internal and output field amplitudes, and the expression (4.24) for the intracavity noise power spectrum, it is convenient to define the output noise power spectrum on the transmission side of the amplifier as

$$N_T(\omega) = \gamma_1\langle n\rangle\frac{\gamma_c(1-C)/\pi}{\omega^2+\gamma_c^2(1-C)^2} . \tag{4.30}$$

This quantity represents the dimensionless mean output flux of noise photons per unit angular frequency bandwidth at frequency $\omega_L+\omega$ per unit time [27]. It resembles a result given in MLS(3.6). The full width of the noise spectrum at half-maximum height is the same as that of the gain profile, given by Γ in (4.9). The total output noise flux on the transmission side of the amplifier is

$$\int d\omega\, N_T(\omega) = \gamma_1\langle n\rangle . \tag{4.31}$$

C. Heterodyne signal-to-noise ratio

The effect of the below-threshold laser amplifier on a coherent input signal is to increase the signal intensity by a gain factor $G_T(\omega)$ in transmission, but also to increase the noise by the chaotic contribution $2\pi N_T(\omega)$. The change in signal-to-noise ratio (SNR) is conveniently described by an "enhancement" factor

$$R(\omega) = \frac{\mathcal{R}_{\text{on}}}{\mathcal{R}_{\text{off}}} , \tag{4.32}$$

which can be larger or smaller than unity, where $\mathcal{R}_{\text{on}}$ ($\mathcal{R}_{\text{off}}$) is the SNR with the amplifier on (off).

In order to calculate the signal-to-noise ratios it is necessary to consider the signal measurement process in some detail. For heterodyne detection with a coherent local oscillator of frequency ω_L whose intensity far exceeds that of the amplified signal, it can be shown [28] that the enhancement factor is given by

$$R(\omega) = \frac{G_T(\omega)}{1+2\eta 2\pi N_T(\omega)} . \tag{4.33}$$

Here the 1 in the denominator arises from shot noise in the detection process, and this contribution remains the same whether the amplifier is on or off. The factor of 2 in the second term appears because both signal and image frequencies of chaotic noise are picked up in ordinary heterodyne detection. The η factor represents the effective quantum efficiency of the detection system, and it takes values between 0 and 1. The factor η must include the intrinsic detector efficiency, and also the effect of any optical losses before the light reaches the detector [28]. (In general terms, η enters the above expressions in the following manner: the efficiency η appears as a linear multiplier in the signal amplitude, and thus reduces signal intensities and their associated gains by a factor of η^2. In the expression for the noise, a factor of η multiplies the shot-noise term, while the additive excess-noise term acquires a factor of η^2.)

It is in principle possible to improve the SNR with the amplifier on by optically filtering out the image frequencies before detection. It is assumed in what follows that this has been done, and the enhancement factor (4.33) then becomes

$$R(\omega) = \frac{G_T(\omega)}{1+\eta 2\pi N_T(\omega)} . \tag{4.34}$$

With insertion of the expressions for the gain and the noise from (4.6) and (4.30), the enhancement factor be-

comes

$$R(\omega)=\frac{\gamma_1\gamma_2}{\omega^2+\gamma_c^2(1-C)^2+2\eta\gamma_1\gamma_c C} . \tag{4.35}$$

For given values of the cavity mirror damping rates γ_1 and γ_2, the factor $R(\omega)$ is maximized for a value of the cooperation parameter given by

$$C=1-\frac{2\eta\gamma_1}{\gamma_1+\gamma_2} \tag{4.36}$$

when the enhancement factor is

$$R(\omega)=\frac{\gamma_1\gamma_2}{\omega^2+\eta\gamma_1[\gamma_1(1-\eta)+\gamma_2]} . \tag{4.37}$$

Consider first the case of perfectly efficient detection with $\eta=1$, when the optimization condition (4.36) is shown by the lowest dashed curve in Fig. 2. It is seen that the SNR is maximized when the amplifier cavity is unsymmetrical, with the lower-transmission mirror facing the detector (that is, $\gamma_1<\gamma_2$). However, even in these optimum conditions, the enhancement factor is less than unity, except for zero detuning where $R(0)=1$. The amplifier cannot therefore produce any improvement in signal-to-noise ratio [21].

However, improvements in the SNR *are* possible when the detection is inefficient. Thus the peak value of the enhancement factor (4.37) can be written as

$$R(0)=1+\frac{(\gamma_2-\eta\gamma_1)(1-\eta)}{\eta[\gamma_1(1-\eta)+\gamma_2]} , \tag{4.38}$$

which is plotted for different values of η in Fig. 3(a). The enhancement factor $R(0)$ is clearly greater than unity when $\eta<1$ and $\eta<\gamma_2/\gamma_1$. The SNR is improved by amplification in this case, and the optimum peak gain obtained from (4.6) and (4.36) is

$$G_T(0)=\gamma_2/\eta^2\gamma_1 . \tag{4.39}$$

D. Intensity-fluctuation noise spectrum

The time-dependent field correlation function calculated in Sec. IV B determines the fringe visibility in a Michelson interference experiment performed on the chaotic light generated by the below-threshold laser. The associated frequency-dependent correlation function controls the noise spectrum in heterodyne detection of the light, as is demonstrated in Sec. IV C. In the present section we briefly consider the corresponding intensity correlation properties. These determine the outcome of "intensity interference" experiments, such as that of Hanbury Brown and Twiss [29], and they also control the noise spectrum in direct detection of the laser light, our main interest here.

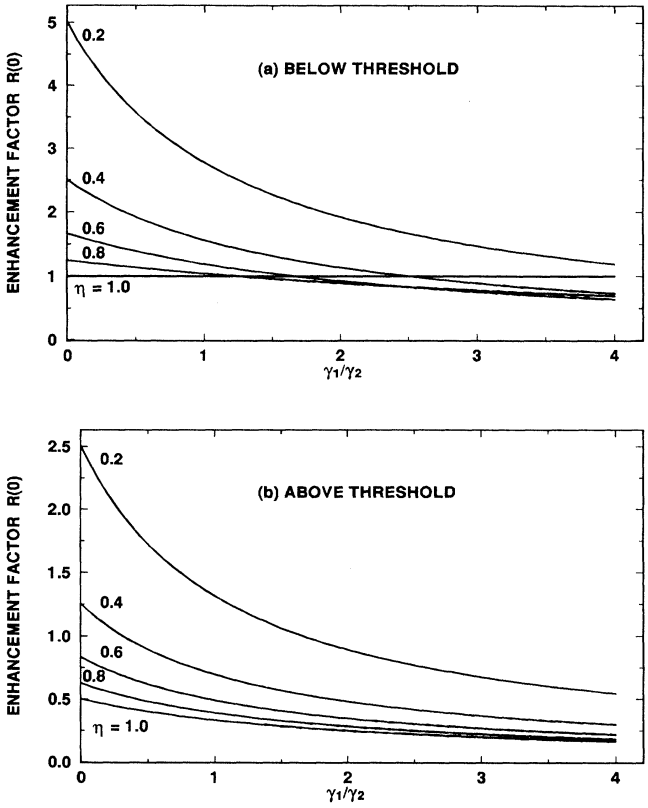

FIG. 3. Peak-enhancement factor $R(0)$ as a function of mirror-decay-rate ratio γ_1/γ_2 for different values of the detection efficiency η. C is assumed to take the value that optimizes the heterodyne signal-to-noise ratio (Fig. 2).

Consider again the light that emerges on the transmission side of the laser-amplifier cavity. Then with further use of the relation (2.4) between internal and output field amplitudes, the intensity noise spectrum is given by [30]

$$S_T(\omega)=\frac{\gamma_1}{2\pi}\langle|\alpha(0)|^2\rangle + \frac{\gamma_1^2}{2\pi}\int_{-\infty}^{\infty}dt\, e^{i\omega t}[\langle|\alpha(0)|^2|\alpha(t)|^2\rangle - \langle|\alpha(0)|^2\rangle^2] , \tag{4.40}$$

where the stationarity property of the field $\alpha(t)$ has been used.

The averages that occur in (4.40) are readily evaluated. Thus from (4.26) and (4.27)

$$\langle|\alpha(0)|^2\rangle=\langle n\rangle=C/(1-C) , \tag{4.41}$$

while use of (4.13) and (4.24) gives

$$\langle|\alpha(0)|^2|\alpha(t)|^2\rangle=\frac{1}{4\pi^2}\int d\omega_1\int d\omega_2\int d\omega_3\int d\omega_4\exp[i(\omega_3-\omega_4)t]\langle\delta\alpha^*(\omega_1)\delta\alpha(\omega_2)\delta\alpha^*(\omega_3)\delta\alpha(\omega_4)\rangle$$
$$=\frac{1}{4\pi^2}\int d\omega_1\int d\omega_2\{1+\exp[i(\omega_2-\omega_1)t]\}\frac{2\gamma_c C}{\omega_1^2+\gamma_c^2(1-C)^2}\frac{2\gamma_c C}{\omega_2^2+\gamma_c^2(1-C)^2} , \tag{4.42}$$

where the pairwise factorization property of the fourth-order correlation function for Gaussian chaotic light has been assumed. The calculation is now easily completed to give an intensity noise spectrum

$$S_T(\omega)=\frac{\gamma_1\langle n\rangle}{2\pi}+\gamma_1^2\langle n\rangle^2\frac{2\gamma_c(1-C)/\pi}{\omega^2+4\gamma_c^2(1-C)^2} \tag{4.43}$$

in agreement with [30]. The second term on the right arises from self-beating of the chaotic field fluctuations whose Lorentzian spectrum is given by (4.30). The self-beating produces a doubled full width at half maximum height of

$$2\Gamma=4\gamma_c(1-C)\ , \tag{4.44}$$

where Γ is defined in (4.9). The first term on the right represents the shot noise produced by the total output photon flux given by (4.31).

V. ABOVE-THRESHOLD LASER AMPLIFIER

The theory and the results of measurements on the gain of the above-threshold laser amplifier have been briefly reported in an earlier paper [1]. There has been much previous work on the corresponding noise properties, with experimental and theoretical studies of the noise dating back to the early years of the laser. Much of this work was concerned with the variation in noise properties with laser pumping rate close to threshold. By contrast, the treatment given in the present section avoids the immediate threshold region. We present a unified theory of the gain and the noise that emphasizes the importance of correlations between signal and image frequencies, apparently overlooked in earlier work. The results for gain and noise are then combined to determine the effect of above-threshold amplification on the signal-to-noise ratio.

A. Gain

The linear amplification of an input signal by an above-threshold laser may be determined by solution of the Maxwell-Bloch equations (2.6), (2.7), and (2.15) for the mean fields in the absence of the Langevin forces Γ. The laser variables $|\alpha_L|$ and D_0 are given by (3.6) and (3.7), while the remaining amplitudes that occur in the trial solutions (2.11), (2.12), and (2.13) all have contributions linear in the input signal field β_S.

Consider first the Maxwell-Bloch equation (2.6) for the internal field. The components of this equation that oscillate at the signal and image frequencies, respectively, give

$$\alpha_S=[(g^2/\gamma_\perp)(\alpha_L D_1+\alpha_S D_0)+\gamma_2^{1/2}\beta_S]/(\gamma_c-i\omega)\ , \tag{5.1}$$

$$\alpha_I=(g^2/\gamma_\perp)(\alpha_L D_1^*+\alpha_I D_0)/(\gamma_c+i\omega)\ , \tag{5.2}$$

where (2.15) has been used. The component of the population inversion at the detuning frequency ω in the Maxwell-Bloch equation (2.7) is

$$D_1=-(2g^2/\gamma_\perp)\times[|\alpha_L|^2D_1+(\alpha_L^*\alpha_S+\alpha_L\alpha_I^*)D_0]/(\gamma_\parallel-i\omega)\ . \tag{5.3}$$

We therefore have three equations for the three unknowns, which are conveniently taken to be α_S, α_I^*, and D_1. The solutions are

$$\alpha_S=-[\omega^2+i\omega\gamma_\parallel C-\gamma_\parallel\gamma_c(C-1)]\gamma_2^{1/2}\beta_S/(i\omega\mathcal{A}_{\rm den})\ , \tag{5.4}$$

$$\alpha_I^*=-\gamma_\parallel\gamma_c(C-1)\gamma_2^{1/2}\beta_S\exp(-2i\phi_L)/(i\omega\mathcal{A}_{\rm den})\ , \tag{5.5}$$

$$D_1=2\gamma_c\gamma_2^{1/2}\alpha_L^*\beta_S/\mathcal{A}_{\rm den}\ , \tag{5.6}$$

with a denominator

$$\mathcal{A}_{\rm den}=\omega^2+i\omega\gamma_\parallel C-2\gamma_\parallel\gamma_c(C-1)\ , \tag{5.7}$$

where ϕ_L is the phase of the laser field so that

$$\alpha_L=|\alpha_L|\exp(i\phi_L)\ . \tag{5.8}$$

The dynamics of the laser in the presence of an input signal are those of a nondegenerate four-wave-mixing process, with the laser excitation of frequency ω_L acting as pump. Thus the coupling of the input signal with the pump produces a modulation of frequency ω in the population inversion (population pulsations [5]). Further coupling between the modulation and the pump generates an optical excitation at the image frequency $\omega_L-\omega$. It is seen from (5.4) and (5.5) that in the degenerate limit of $\omega\to 0$, $\alpha_L^*\alpha_S$ and $\alpha_L\alpha_I^*$ are nearly equal in magnitude but opposite in sign. The signal and image amplitudes remain comparable in magnitude as the detuning increases from zero until ω is greater than γ_c and/or $\gamma_\parallel$ when the signal amplitude exceeds that of the image. The signal excitation is completely dominant for detunings much greater than the decay rates.

The definition of the gain for the above-threshold laser amplifier depends upon the extent to which both signal and image frequencies are detected in the amplifier outputs. Suppose first that the signal and image frequencies can be observed separately. These arrangements correspond, respectively, to phase-preserving and phase-conjugating linear amplification [21]. The intensity gains in transmission obtained with the use of (5.4) and (5.5) are

$$G_{TS}(\omega)=\gamma_1\left|\frac{\alpha_S}{\beta_S}\right|^2=\frac{\gamma_1\gamma_2}{\omega^2}\frac{\omega^2\gamma_\parallel^2C^2+[\omega^2-\gamma_\parallel\gamma_c(C-1)]^2}{\mathcal{D}_{\rm den}} \tag{5.9}$$

and

$$G_{TI}(\omega)=\gamma_1\left|\frac{\alpha_I}{\beta_S}\right|^2=\frac{\gamma_1\gamma_2}{\omega^2}\frac{\gamma_\parallel^2\gamma_c^2(C-1)^2}{\mathcal{D}_{\rm den}}\ , \tag{5.10}$$

where the common denominator is

$$\mathcal{D}_{\rm den}=|\mathcal{A}_{\rm den}|^2=\omega^2\gamma_\parallel^2C^2+[\omega^2-2\gamma_\parallel\gamma_c(C-1)]^2\ . \tag{5.11}$$

Some representative gain profiles are shown in Fig. 4 with the common divergent forms

$$G_{TS}(\omega)\approx G_{TI}(\omega)\approx\gamma_1\gamma_2/4\omega^2\ ,\quad \omega\ll\gamma_c,\gamma_\parallel \tag{5.12}$$

clearly visible at small detunings. The divergent gains are consistent with the expectation from injection-locking studies [11].

These separate gains are not in fact ordinarily observed in the straightforward arrangement where the amplifier output light falls on a photodetector without any intermediate filtering. The measured output flux in this case is obtained from (2.4) and (2.11) in the form

$$|\alpha_{\text{out}}|^2=\gamma_1|\alpha|^2$$
$$=\gamma_1[\,|\alpha_L|^2+(\alpha_L^*\alpha_S+\alpha_L\alpha_I^*)\exp(-i\omega t)+\text{c.c.}\,]\ , \tag{5.13}$$

correct to first order in β_S. The experiment thus observes simultaneously the self-heterodyne beats between the strong laser beam, acting as local oscillator, and the signal and image beams. The signal and image contributions are indistinguishable in this arrangement. The corresponding heterodyne beat obtained by superposition of

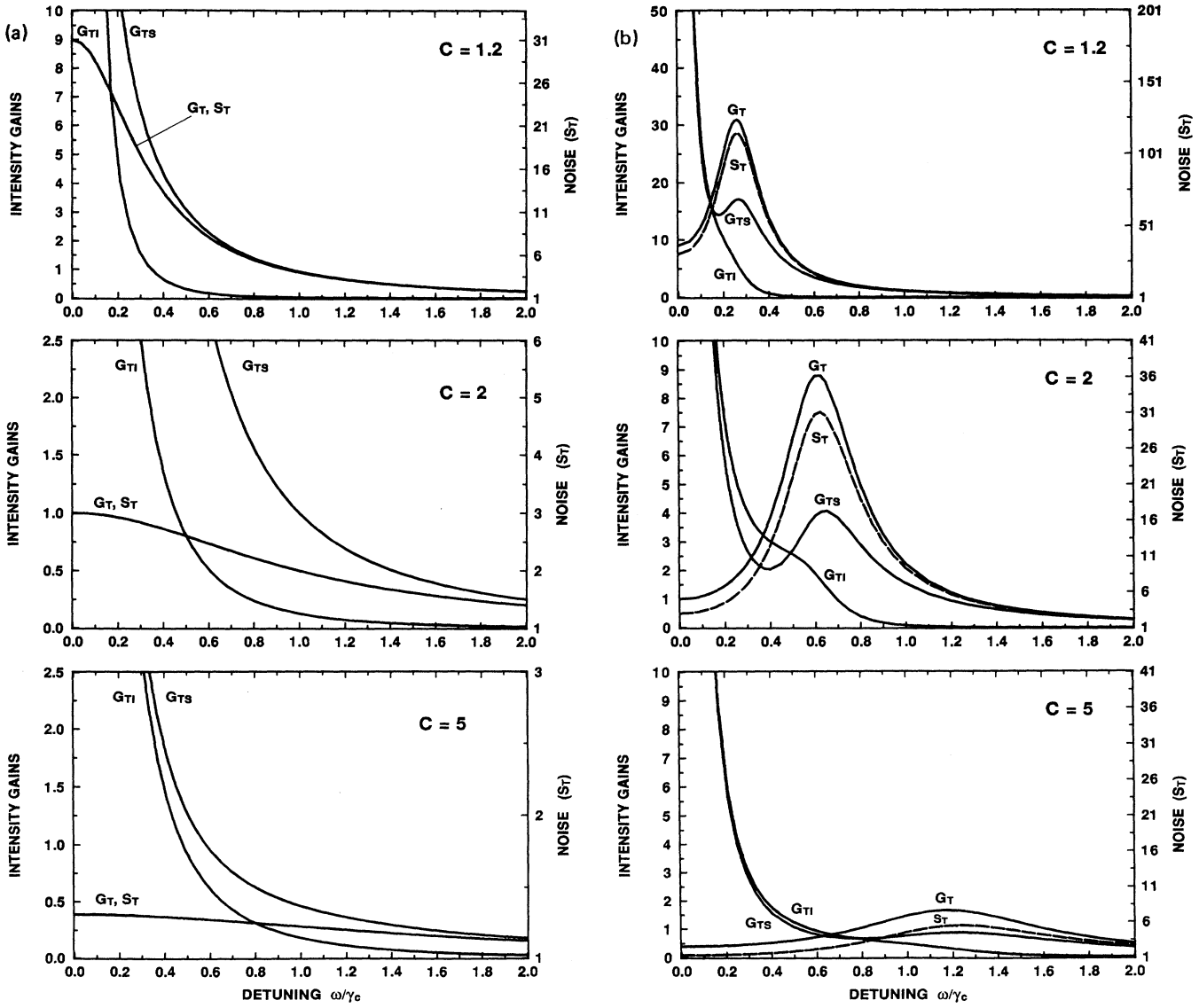

FIG. 4. Gain and noise profiles for the above-threshold amplifier with symmetrical mirror losses ($\gamma_1=\gamma_2$) for "low" (top), "medium," and "high" laser power. Note the differences in vertical scale between the plots, and also between gain and noise. The noise $S_T(\omega)$ is expressed in units of the shot noise. The plots in (a) represent a class-A laser ($\gamma_\parallel\gg\gamma_c$) for which the heterodyne gain (G_T) and the noise (S_T) have the same shape. This is not the case for the plots in (b) for the class-B laser (e.g., CO_2) with $\gamma_\parallel/\gamma_c=0.2$. The noise spectra are given here by the dashed curves.

the laser beam with the unamplified input signal is

$$\gamma_1^{1/2}\alpha_L^*\beta_S \exp(-i\omega t)+\text{c.c.} \tag{5.14}$$

The complex amplitude gain in transmission for the experiment considered here is therefore

$$g_T=\gamma_1^{1/2}(\alpha_L^*\alpha_S+\alpha_L\alpha_I^*)/\alpha_L^*\beta_S \ . \tag{5.15}$$

The explicit form of the gain is now easily obtained by substitution of (5.4) and (5.5) into (5.15) with the result

$$g_T=i(\gamma_1\gamma_2)^{1/2}(\omega+i\gamma_\parallel C)/\mathscr{A}_{\text{den}} \ , \tag{5.16}$$

where the denominator is given by (5.7). The corresponding intensity transmission gain is

$$G_T(\omega)=|g_T|^2=\frac{\gamma_1\gamma_2(\omega^2+\gamma_\parallel^2C^2)}{\omega^2\gamma_\parallel^2C^2+[\omega^2-2\gamma_\parallel\gamma_c(C-1)]^2} \ , \tag{5.17}$$

with the denominator from (5.11) written out in full. The zero-detuning gain is accordingly

$$G_T(0)=\gamma_1\gamma_2C^2/4\gamma_c^2(C-1)^2 \ , \tag{5.18}$$

and this is greater than unity for

$$C<(\gamma_1+\gamma_2)/[\gamma_1-(\gamma_1\gamma_2)^{1/2}+\gamma_2] \ . \tag{5.19}$$

The upper part of the shaded region in Fig. 2 shows the parameter values corresponding to gains greater than unity. An expression for the gain has been derived by Pantell [13] using a theory that neglected from the outset any excitation of image frequencies. His expression differs from (5.17) by the factor of 2 in the denominator.

Examples of the heterodyne gain profile (5.17) are included in Fig. 4. It is seen that the cancellation of the divergent parts of the separate signal and image gains at small detunings leaves a well-behaved composite gain profile $G_T(\omega)$. The gain function always has a turning point at $\omega=0$, but this can be either a maximum or minimum depending on the values of the laser parameters. It is found by differentiation of (5.17) that the gain is a minimum at $\omega=0$ when

$$\gamma_\parallel<2(1+2^{1/2})\gamma_c(C-1)/C^2 \ , \tag{5.20}$$

and peak gain then appears at a nonzero detuning given by

$$\omega_{\max}^2=-\gamma_\parallel^2C^2+2\gamma_\parallel\{\gamma_c(C-1)[\gamma_\parallel C^2+\gamma_c(C-1)]\}^{1/2} \ . \tag{5.21}$$

This somewhat-complicated expression simplifies in the limit where the laser parameters satisfy the condition $\gamma_\parallel \ll \gamma_c$ when

$$\omega_{\max}=\pm[2\gamma_\parallel\gamma_c(C-1)]^{1/2}=\pm2\gamma_c|\alpha_L|/D_0^{1/2} \ , \tag{5.22}$$

where (3.7) to (3.9) have been used. These frequencies of peak gain are the same as the frequencies that occur in theories of the relaxation oscillations associated with the spiking behavior found in most solid-state and some gas lasers [11]. The gain at the frequency $\omega_{\max}$, obtained by substitution of (5.22) into (5.17), is $G_T(\omega_{\max})=\gamma_1\gamma_2/\gamma_\parallel^2C^2$. Note that this gain is high, and that values greater than unity persist even at high pumping rates ($C\gg1$). The corresponding signal and image gains (G_{TS} and G_{TI}) from (5.9) and (5.10) are equal, and they each take values of one quarter of G_T. Hence, their contributions must add in phase to produce the combined heterodyne gain G_T. In this case, the signal and image sidebands lead to pure amplitude modulation; in other words, the input resonantly excites the natural relaxation oscillation of the laser.

The above discussion refers to the gains measured in transmission through the laser amplifier. The corresponding amplitude gain measured in reflection, when both signal and image frequencies are detected, is defined by

$$g_R=\frac{\gamma_2^{1/2}(\alpha_L^*\alpha_S+\alpha_L\alpha_I^*)}{\alpha_L^*\beta_S}-1 \ . \tag{5.23}$$

The explicit form obtained by substitution from (5.4) and (5.5) is

$$g_R=\frac{i\gamma_2(\omega+i\gamma_\parallel C)}{\mathscr{A}_{\text{den}}}-1 \ , \tag{5.24}$$

where the denominator is defined in (5.7).

The results derived so far apply to both class-A and class-B lasers, and we shall show that they provide a good description of gain measurements made on CO_2 lasers in the B category. We also present measurements on Ar^+ lasers, which belong to the A category with $\gamma_c \ll \gamma_\parallel$. Most of the theoretical results simplify considerably in this case, and we conclude the section with a discussion of the class-A gain characteristics.

Taking then $\gamma_c \ll \gamma_\parallel$ for the remainder of the section, the field amplitudes (5.4) and (5.5) simplify to

$$\alpha_S=-\frac{[i\omega C-\gamma_c(C-1)]\gamma_2^{1/2}\beta_S}{i\omega[i\omega C-2\gamma_c(C-1)]} \tag{5.25}$$

and

$$\alpha_I^*=-\frac{\gamma_c(C-1)\gamma_2^{1/2}\beta_S\exp(-2i\phi_L)}{i\omega[i\omega C-2\gamma_c(C-1)]} \ . \tag{5.26}$$

The intensity transmission gains for measurements on the signal and image frequencies alone thus simplify from the expressions (5.9) and (5.10) to

$$G_{TS}(\omega)=\frac{\gamma_1\gamma_2}{\omega^2}\frac{\omega^2C^2+\gamma_c^2(C-1)^2}{\omega^2C^2+4\gamma_c^2(C-1)^2} \tag{5.27}$$

and

$$G_{TI}(\omega)=\frac{\gamma_1\gamma_2}{\omega^2}\frac{\gamma_c^2(C-1)^2}{\omega^2C^2+4\gamma_C^2(C-1)^2} \ . \tag{5.28}$$

The forms of these separate gain profiles are shown in Fig. 4(a).

The understanding of the amplifier characteristics for measurements in which the signal and image contributions are detected simultaneously is helped by a consideration of the two complex components in the amplitude transmission gain (5.15). These are illustrated in

Fig. 5 together with their sum. The relative phase ϕ of the signal and image components is given by

$$\tan\phi = -\omega C/\gamma_c(C-1)\ , \tag{5.29}$$

and this angle varies between π and $\pi/2$ as the detuning ω increases from a value much smaller than γ_c to a value much larger than γ_c. It follows by the theorem of Pythagoras from the geometry of Fig. 5 that

$$|\alpha_L^* \alpha_S + \alpha_L \alpha_I^*|^2 = |\alpha_L^* \alpha_S|^2 - |\alpha_L \alpha_I^*|^2\ , \tag{5.30}$$

and the various transmission gains are therefore related by

$$\begin{aligned} G_T(\omega) &= G_{TS}(\omega) - G_{TI}(\omega) \\ &= \frac{\gamma_1\gamma_2}{\omega^2 + [2\gamma_c(C-1)/C]^2}\ . \end{aligned} \tag{5.31}$$

The zero-detuning gain given by (5.18) is now the peak value and the condition (5.19) must be satisfied for amplification to occur. The full width of the gain profile at half maximum height is

$$\Gamma = 4\gamma_c(C-1)/C = 2\Gamma_0(C-1)/C\ . \tag{5.32}$$

The form of the gain profile (5.31) and its relation to the signal and image contributions is illustrated in Fig. 4(a).

The expressions (4.6) and (5.31) for the amplifier gains below and above threshold conform with the identification of the laser threshold as the analog of a second-order phase transition [5,12,31]. Thus the zero-detuning gains (4.7) and (5.18) have exactly the forms expected for the squares of the zero-field susceptibilities below and above threshold, with strong similarities to the squares of the zero-field susceptibilities of a ferromagnet above and below its Curie temperature. The bandwidths (4.9) and (5.32) are related by the replacement $C \to 1/C$ and the insertion of an additional factor of 2 above threshold. The bandwidths tend to zero as threshold is approached from below or above, analogous to the critical slowing down at a second-order phase transition. The variations of the zero-detuning gain and the gain bandwidth with cooperation parameter C are shown in Fig. 6.

The amplitude gain in reflection given by (5.24) simplifies in the limit $\gamma_c \ll \gamma_\parallel$ to

$$g_R = -\frac{(i\omega-\gamma_1)C+2\gamma_c}{(i\omega-2\gamma_c)C+2\gamma_c}\ . \tag{5.33}$$

The corresponding intensity gain is

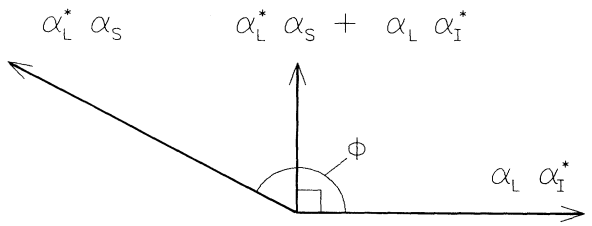

FIG. 5. Complex vector diagram of signal and image fields showing relative phase angle ϕ.

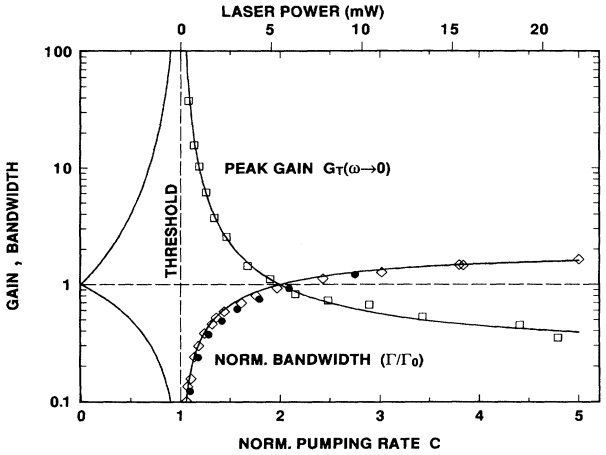

FIG. 6. Above-threshold amplifier gain and bandwidth as functions of laser pumping rate C for the Ar^+ laser (class A). □, peak gain measurement; ◇, gain bandwidth measurement; ●, noise bandwidth measurement. Solid curves below threshold: theory (Sec. IV). Curves above threshold: theory (Sec. V).

$$\begin{aligned} G_R(\omega) &= \frac{\omega^2C^2 + (2\gamma_c - \gamma_1 C)^2}{\omega^2C^2 + 4\gamma_c^2(C-1)^2} \\ &= 1 + \frac{\gamma_2 C[2(\gamma_1+\gamma_2) - (2\gamma_1+\gamma_2)C]}{\omega^2C^2 + 4\gamma_c^2(C-1)^2}\ , \end{aligned} \tag{5.34}$$

which is of the form 1 ± (a Lorentzian function). Note that

$$G_R(\omega) = 1 \quad \text{for } C = 2(\gamma_1+\gamma_2)/(2\gamma_1+\gamma_2)\ , \tag{5.35}$$

and the reflection gain is greater than unity for smaller values of C. For a symmetrical cavity ($\gamma_1 = \gamma_2 = \gamma_c$), the gain may be written as

$$G_R(\omega) = 1 + \frac{\gamma_c^2 C(4-3C)}{\omega^2C^2 + 4\gamma_c^2(C-1)^2}\ . \tag{5.36}$$

Some examples of this function are plotted in Fig. 7. Two special cases are notable: when $C = \frac{4}{3}$, the response is flat and the gain is unity. For $C = 2$, the gain at zero detuning $G_R(0) = 0$. Note that this does not imply that no light is reflected; rather, that signal and image contributions precisely cancel.

B. Noise

We use again the Maxwell-Bloch equations (2.6), (2.7), and (2.15) with the forces Γ_D and Γ_d retained but the signal amplitude β_{in} set equal to zero. The mean laser field amplitude is given by (3.6) but its undetermined phase angle is subjected to the usual diffusion process. Thus in contrast to the below-threshold ansatz (4.13), we look for zero-mean fluctuations in the field by setting

$$\alpha(t) = [|\alpha_L| + \delta\alpha(t)]\exp[i\delta\phi(t) - i\omega_L t]\ , \tag{5.37}$$

where $\delta\alpha(t)$ and $\delta\phi(t)$ are real and dimensionless amplitude and phase fluctuations, respectively. The population

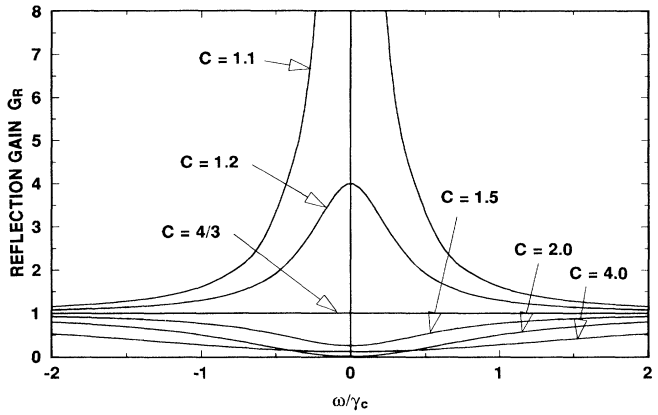

FIG. 7. Theoretical profiles for reflection gain of an Ar^+ laser (class A) at different levels of laser power for a symmetrical cavity ($\gamma_1=\gamma_2$).

inversion is assigned a fluctuating contribution in addition to its mean value D_0 given by (3.7),

$$D(t)=D_0+\delta D(t) . \tag{5.38}$$

These trial solutions are now substituted into the Maxwell-Bloch equations, and the terms of the first order in the fluctuating variables and forces give

$$\delta\dot{\alpha}(t)+i|\alpha_L|\delta\phi(t)-(g^2|\alpha_L|/\gamma_\perp)\delta D(t) =(g/\gamma_\perp)\Gamma_d(t)\exp[-i\delta\phi(t)+i\omega_L t] \tag{5.39}$$

and

$$\delta\dot{D}(t)+\gamma_\parallel C\delta D(t)+4\gamma_c|\alpha_L|\delta\alpha(t) =-(g|\alpha_L|/\gamma_\perp)\{\Gamma_d(t)\exp[-i\delta\phi(t)+i\omega_L t] +\text{c.c.}\}+\Gamma_D(t) . \tag{5.40}$$

It will transpire that the force $\Gamma_d(t)$ contributes to the final results only in correlation with its complex conjugate. In addition, the phase fluctuations represented by $\delta\phi(t)$ vary on a time scale that is usually very long compared to the time scale of the randomly fluctuating force $\Gamma_d(t)$, except very close to threshold. It is therefore an excellent approximation to remove the phase fluctuation from the right-hand sides of (5.39) and (5.40).

With this approximation, and with Fourier transforms defined in the manner of (4.17), the real and imaginary parts of (5.39) produce the pair of transformed equations

$$-i\omega\delta\alpha(\omega)-(g^2|\alpha_L|/\gamma_\perp)\delta D(\omega) =(g/2\gamma_\perp)[\Gamma_d(\omega_L+\omega)+\Gamma_d^*(\omega_L-\omega)] \tag{5.41}$$

and

$$-i\omega\delta\phi(\omega)=-i(g/2\gamma_\perp|\alpha_L|)[\Gamma_d(\omega_L+\omega) -\Gamma_d^*(\omega_L-\omega)] , \tag{5.42}$$

while (5.40) transforms to

$$-i\omega\delta D(\omega)+\gamma_\parallel C\delta D(\omega)+4\gamma_c|\alpha_L|\delta\alpha(\omega) =(g|\alpha_L|/\gamma_\perp)[\Gamma_d(\omega_L+\omega)+\Gamma_d^*(\omega_L-\omega)]+\Gamma_D(\omega) . \tag{5.43}$$

These are three simultaneous equations for the three kinds of fluctuation variable and their solutions are

$$\delta\alpha(\omega)=\{(g/2\gamma_\perp)(i\omega-\gamma_\parallel)[\Gamma_d(\omega_L+\omega)+\Gamma_d^*(\omega_L-\omega)] -(g^2|\alpha_L|/\gamma_\perp)\Gamma_D(\omega)\}/\mathcal{A}_{\text{den}} , \tag{5.44}$$

$$\delta\phi(\omega)=(g/2\omega\gamma_\perp|\alpha_L|)[\Gamma_d(\omega_L+\omega)-\Gamma_d^*(\omega_L-\omega)] , \tag{5.45}$$

and

$$\delta D(\omega)=\{-(g|\alpha_L|/\gamma_\perp)(i\omega-2\gamma_c)[\Gamma_d(\omega_L+\omega) +\Gamma_d^*(\omega_L-\omega)] +i\omega\Gamma_D(\omega)\}/\mathcal{A}_{\text{den}} , \tag{5.46}$$

where the denominator is given by (5.7).

The Langevin force correlation functions that are needed to evaluate the power spectra of the three kinds of fluctuation are again obtained from the results of Louisell [10]. The only force correlations of significant magnitude are given by

$$\langle\Gamma_d^*(\omega_L+\omega)\Gamma_d(\omega_L+\omega')\rangle=2\gamma_\perp D_0\delta(\omega-\omega') \tag{5.47}$$

and

$$\langle\Gamma_D(\omega)\Gamma_D(\omega')\rangle=2\gamma_\parallel D_0\delta(\omega+\omega') . \tag{5.48}$$

The required noise power spectra are therefore

$$\langle\delta\alpha(\omega)\delta\alpha(\omega')\rangle=\gamma_c(\omega^2+\gamma_\parallel^2 C)\delta(\omega+\omega')/\mathcal{D}_{\text{den}} , \tag{5.49}$$

$$\langle\delta\phi(\omega)\delta\phi(\omega')\rangle=(\gamma_c/\omega^2|\alpha_L|^2)\delta(\omega+\omega') , \tag{5.50}$$

and

$$\langle\delta D(\omega)\delta D(\omega')\rangle=2\gamma_\perp\gamma_\parallel\gamma_c[\omega^2 C+4\gamma_c^2(C-1)] \times\delta(\omega+\omega')/(g^2\mathcal{D}_{\text{den}}) , \tag{5.51}$$

where the denominator is given by (5.11). Note that each of these spectra involves correlations between pairs of frequencies with equal and opposite detuning from the laser frequency ω_L.

The time-dependent field correlation function is obtained from (5.37) in the form

$$\langle\alpha^*(t)\alpha(t')\rangle=\{|\alpha_L|^2+\langle\delta\alpha(t)\delta\alpha(t')\rangle\} \times\langle\exp\{i[\delta\phi(t')-\delta\phi(t)]\}\rangle \times\exp[i\omega_L(t-t')] . \tag{5.52}$$

Consider first the phase angle average, which is evaluated by a standard procedure according to

$$\langle \exp\{i[\delta\phi(t')-\delta\phi(t)]\}\rangle = \left\langle \exp\left[i\int_t^{t'} d\tau\,\delta\dot{\phi}(\tau)\right]\right\rangle$$
$$= \exp\left[-\tfrac{1}{2}\left\langle\left[\int_t^{t'} d\tau\,\delta\dot{\phi}(\tau)\right]^2\right\rangle\right]$$
$$= \exp\left[-\tfrac{1}{2}\int_t^{t'} d\tau\int_t^{t'} d\tau'\langle\delta\dot{\phi}(\tau)\delta\dot{\phi}(\tau')\rangle\right] . \quad (5.53)$$

The required correlation function is obtained by Fourier transformation of (5.50) as

$$\langle\delta\dot{\phi}(\tau)\delta\dot{\phi}(\tau')\rangle = (\gamma_c/|\alpha_L|^2)\delta(\tau-\tau') , \quad (5.54)$$

and the phase angle average is therefore

$$\langle\exp\{i[\delta\phi(t')-\delta\phi(t)]\}\rangle = \exp(-\gamma_c|t-t'|/2|\alpha_L|^2) . \quad (5.55)$$

The amplitude average in (5.52) is similarly evaluated by Fourier transformation of (5.49). The average is somewhat complicated in general, and we consider here only the result for class-A lasers where $\gamma_c \ll \gamma_\parallel$ and (5.49) reduces to

$$\langle\delta\alpha(\omega)\delta\alpha(\omega')\rangle = \frac{\gamma_c C}{\omega^2C^2+4\gamma_c^2(C-1)^2}\delta(\omega+\omega') . \quad (5.56)$$

The Fourier transform is now readily evaluated to give

$$\langle\delta\alpha(t)\delta\alpha(t')\rangle = \frac{\exp[-2\gamma_c(C-1)|t-t'|/C]}{4(C-1)} . \quad (5.57)$$

These amplitude fluctuations decay with a much shorter time scale than do the phase fluctuations, and the field correlation function (5.52) can be written as

$$\langle\alpha^*(t)\alpha(t')\rangle = \left[|\alpha_L|^2\exp(-\gamma_c|t-t'|/2|\alpha_L|^2) + \frac{\exp[-2\gamma_c(C-1)|t-t'|/C]}{4(C-1)}\right] \times \exp[i\omega_L(t-t')] \quad (5.58)$$

to a very good approximation.

The field correlation function (5.58) has a form similar to a result derived by Risken [32]. It represents an intracavity excitation of $|\alpha_L|^2$ laser photons plus a much smaller noise contribution of mean photon number $1/4(C-1)$. The corresponding output spectrum on the transmission side of the laser amplifier in units of photon flux per unit angular frequency bandwidth can be written as a sum of two contributions. The first contribution is

$$L_T(\omega) = \gamma_1|\alpha_L|^2\frac{\gamma_c/2\pi|\alpha_L|^2}{\omega^2+(\gamma_c/2|\alpha_L|^2)^2} , \quad (5.59)$$

where ω is the detuning from the laser frequency ω_L. This represents the intense laser flux, with a very narrow bandwidth

$$\Gamma_L = \gamma_c/|\alpha_L|^2 \quad (5.60)$$

caused by the phase diffusion effect (the well-known Schawlow-Townes linewidth [11,20,33)]. It is seen by comparison with (4.28) that, as a function of the inverse intracavity photon number, the bandwidth is *reduced* by a factor of 2 as the laser is taken from just below to just above threshold at $C=1$. Evidence in support of this factor-of-2 reduction in bandwidth has been obtained from measurements with a Michelson interferometer [34]. The second contribution,

$$N_T(\omega) = \frac{\gamma_1}{4(C-1)}\frac{2\gamma_c(C-1)/\pi C}{\omega^2+[2\gamma_c(C-1)/C]^2} , \quad (5.61)$$

represents the weak amplitude-fluctuation noise flux, with a much broader bandwidth

$$\Gamma_N = 4\gamma_c(C-1)/C . \quad (5.62)$$

The noise bandwidth is thus identical to the gain bandwidth (5.32) for an above-threshold class-A laser. It is seen by comparison of (5.61) with (4.30) that, in addition to the replacement of C by $1/C$, the noise bandwidth is *increased* by a factor of 2 as the laser is taken from below to above threshold.

The noise flux (5.61) is usually very much smaller than the coherent laser flux (5.59), and it can be neglected in calculations of the laser output intensity. The amplitude-fluctuation noise must, however, be retained for calculations of the intensity-fluctuation spectrum, where it provides the main addition to the shot-noise component. Note that this small amplitude-fluctuation noise contribution differs from the below-threshold chaotic noise, which suffers both large phase *and* amplitude fluctuations.

C. Direct-detection signal-to-noise ratio

The effect of the above-threshold laser amplifier on a coherent input signal is to increase the signal intensity by a gain factor $G_T(\omega)$ in transmission, but to increase the noise by the amplitude-fluctuation component in $N_T(\omega)$. The change in signal-to-noise ratio is again conveniently described by the enhancement factor $R(\omega)$ defined in (4.32).

In our treatment of the below-threshold laser amplifier, we considered the SNR in heterodyne detection in Sec. IV C and the intensity noise spectrum for direct detection in Sec. IV D. These two kinds of detection lose their distinction for the above-threshold laser amplifier. Thus in direct detection of the amplifier output the intense laser light, represented by (5.59), acts as a local oscillator for detection of the amplified signal and the amplitude fluctuation noise represented by (5.61). Direct detection is therefore equivalent to a form of self-heterodyne-detection. In the present section we first derive the

intensity-fluctuation noise spectrum and then use the result to evaluate the SNR enhancement factor.

The intensity noise spectrum is obtained from (4.40) with substitution of the form of the internal field from (5.37). The phase-fluctuation terms cancel, and the spectrum correct to first order in the laser intensity is

$$S_T(\omega)=\frac{\gamma_1|\alpha_L|^2}{2\pi}+\frac{\gamma_1^2}{2\pi}4|\alpha_L|^2\int dt\,\exp(i\omega t)\times\langle\delta\alpha(t)\delta\alpha(0)\rangle\ . \tag{5.63}$$

The factor of 4 that appears in the second term represents a doubling of the contribution of the amplitude-fluctuation noise compared to the contribution of an equivalent excitation of ordinary chaotic light. The integration is readily performed with the use of (5.49) to give

$$S_T(\omega)=\frac{\gamma_1|\alpha_L|^2}{2\pi}+\gamma_1^2|\alpha_L|^2\frac{2\gamma_c(\omega^2+\gamma_\parallel^2C)/\pi}{\omega^2\gamma_\parallel^2C^2+[\omega^2-2\gamma_\parallel\gamma_c(C-1)]^2}\ . \tag{5.64}$$

The first term on the right-hand side is the shot noise and the second term arises from the beating of the coherent laser beam with the amplitude-fluctuation noise. It is seen that this term has the same denominator as the transmission gain given by (5.17), and hence for sufficiently small $\gamma_\parallel$ the noise spectrum likewise has a minimum at $\omega=0$ and a displaced maximum at the relaxation oscillation frequency in (5.22). The corresponding intensity-fluctuation noise spectra are plotted alongside the gain in Fig. 4. Similar intensity-fluctuation spectra have been derived and illustrated for application to solid-state [20] and semiconductor [7] lasers, following earlier work on more general laser systems [35,36]. The relaxation-oscillation noise sidebands are a familiar feature of semiconductor laser spectra [6].

We now consider the signal-to-noise ratio for the above-threshold laser amplifier, with the discussion limited to class-A lasers for which $\gamma_c\ll\gamma_\parallel$. The transmission gain is then given by (5.31) and the noise (5.64) reduces to

$$S_T(\omega)=\frac{\gamma_1|\alpha_L|^2}{2\pi}+\frac{\gamma_1^2|\alpha_L|^2}{C-1}\frac{2\gamma_c(C-1)/\pi C}{\omega^2+[2\gamma_c(C-1)/C]^2}=\frac{\gamma_1|\alpha_L|^2}{2\pi}+4\gamma_1|\alpha_L|^2N_T(\omega) \tag{5.65}$$

in agreement with [30]. The enhancement factor $R(\omega)$ from (4.32) is calculated on the assumption that the "amplifier-off" measurement refers to heterodyne detection of the input signal with a local oscillator flux equal to $\gamma_1|\alpha_L|^2$. Then

$$R(\omega)=\frac{\gamma_1\gamma_2}{\omega^2+[2\gamma_c(C-1)/C]^2+(\eta\gamma_1 4\gamma_c/C)}\ , \tag{5.66}$$

where η is again the detection quantum efficiency and enters the gain and noise expressions in an identical fashion to the below-threshold regime. For given values of the cavity mirror damping rates γ_1 and γ_2, the factor $R(\omega)$ is maximized for a value of the cooperation parameter given by

$$C=1+\frac{\eta\gamma_1}{\gamma_1(1-\eta)+\gamma_2} \tag{5.67}$$

when the enhancement factor is

$$R(\omega)=\frac{\gamma_1\gamma_2}{\omega^2+\eta\gamma_1[\gamma_1(2-\eta)+2\gamma_2]}\ . \tag{5.68}$$

Consider first the case of perfectly efficient detection with $\eta=1$, when the optimization condition (5.67) is shown by the uppermost dashed line in Fig. 2. It is seen that the SNR is again maximized when the amplifier cavity is unsymmetrical with the lower-transmission mirror facing the detector. However, even in these optimum conditions, the largest value of the enhancement factor, achieved for zero detuning, is $R(0)=\frac{1}{2}$. This factor-of-2 degradation in the SNR is the standard result found for high-gain amplification of coherent light [21].

Improvements in SNR are again possible, however, when the detection is inefficient with a sufficiently small η. Thus the peak value of the enhancement factor (5.68) can be written as

$$R(0)=1+\frac{\gamma_2(1-2\eta)-\eta\gamma_1(2-\eta)}{\eta[\gamma_1(2-\eta)+2\gamma_2]}\ , \tag{5.69}$$

and this is plotted in Fig. 3(b). The enhancement is greater than unity when $\gamma_2(1-2\eta)>\eta\gamma_1(2-\eta)$. Thus η must be less than one half for there to be any possibility of SNR improvement. The optimum peak gain obtained from (5.31) and (5.67) is identical to the expression (4.39), which is therefore valid both below and above threshold.

For an amplifier that has a symmetrical cavity with $\gamma_1=\gamma_2=\gamma_c$, the zero-detuning enhancement factor obtained from (5.66) is

$$R(0)=C^2/4[C^2-(2-\eta)C+1]\ . \tag{5.70}$$

Thus for perfectly efficient detection, the enhancement factor increases from $\frac{1}{4}$ at $C=1$ to $\frac{1}{3}$ at $C=2$.

It was shown in Sec. IV C that degradation in the heterodyne SNR for the below-threshold amplifier can be avoided, at least for perfectly efficient detection and small detunings, by optical filtering of the image frequencies before detection. It might be thought that such filtering would also be advantageous for the above-threshold amplifier, particularly for class-A lasers where the gain $G_{TS}(\omega)$ for detection of the signal frequencies alone always exceeds the combined signal and image gain $G_T(\omega)$, as shown in Fig. 4(a). However, image-band filtering unfortunately increases not only the gain but also the noise, since it removes noise-cancellation effects of correlations between the signal and image fluctuations, analogous to the gain cancellation described by (5.31). Equivalently, the noise increases because the filtered detection picks up a contribution from the phase fluctuations in the laser

flux $L_T(\omega)$ given by (5.59), in addition to the contribution from the amplitude-fluctuation noise flux $N_T(\omega)$ given by (5.61). Observations and interpretation of the noise-cancellation effect have been reported previously [3] for the subthreshold modes on either side of a single Ar^+ laser mode, where filtering of the image side of the narrow lasing mode itself is not possible in practice (see [37] for related measurements on semiconductor lasers). We conclude the present section with some remarks on the effects of noise filtering based on these observations and their detailed theory [38].

Consider an experiment in which the image frequencies are completely filtered out for detunings greater than ω_f, such that the laser flux $L_T(\omega)$ almost entirely passes through but the noise flux $N_T(\omega)$ is almost entirely removed. The filter cutoff frequency must therefore satisfy

$$\gamma_c/2|\alpha_L|^2 \ll \omega_f \ll 2\gamma_c(C-1)/C \ . \tag{5.71}$$

The intensity noise spectrum for the resulting detection of signal frequencies alone for $\omega > \omega_f$ is given by [38]

$$S_{TS}(\omega)=\frac{\gamma_1|\alpha_L|^2}{2\pi}+\gamma_1^2|\alpha_L|^2\left[\frac{\gamma_c/2\pi}{\omega^2}+\frac{1}{4(C-1)}\frac{2\gamma_c(C-1)/\pi C}{\omega^2+[2\gamma_c(C-1)/C]^2}\right]$$
$$=\frac{\gamma_1|\alpha_L|^2}{2\pi}+\gamma_1|\alpha_L|^2[L_T(\omega)+N_T(\omega)] \ . \tag{5.72}$$

It is seen by comparison with (5.65) that the first, shot-noise contribution on the right is unchanged and the amplitude noise is reduced by a factor of 4, but there is now a new phase-noise contribution. The enhancement factor defined in (4.32) becomes

$$R(\omega)=\frac{G_{TS}(\omega)}{1+\eta 2\pi[L_T(\omega)+N_T(\omega)]} \ , \tag{5.73}$$

and this can be written in terms of the laser parameters with the use of (5.27) and (5.72). The enhancement factor takes its largest value for small detunings (but with ω still assumed larger than ω_f), where it tends to

$$R(0)=\gamma_2/2\eta(\gamma_1+\gamma_2) \ . \tag{5.74}$$

For perfectly efficient detection, this again has a maximum value of $R(0)=\frac{1}{2}$, achieved for $\gamma_1 \ll \gamma_2$, in accordance with standard amplifier theory [21], but improvements in SNR are possible for sufficiently inefficient detection, this time when

$$\eta < \gamma_2/2(\gamma_1+\gamma_2) \ . \tag{5.75}$$

These results show that no general improvement in direct detection SNR can be achieved by image-band filtering.

VI. ABOVE-THRESHOLD LASER AMPLIFIER: EXPERIMENTAL MEASUREMENTS OF GAIN AND NOISE

In this section we describe a straightforward but powerful technique for the experimental measurement of gain in an above-threshold laser amplifier, discussed briefly in [1]. Data have been obtained for class-*A* [argon-ion (Ar^+)] and class-*B* (CO_2) lasers, and these results are compared with the theoretical predictions of the preceding section. Data have also been obtained for the intensity-fluctuation noise spectrum of the Ar^+ laser, allowing a direct comparison of gain and noise bandwidths.

Figure 8(a) shows the experimental arrangement, used for study of the Ar^+-laser gain characteristics. The laser is a Lexel Model 95, modified for double-ended output, with both mirrors having approximately 95% reflectivity. At the relatively low pumping rates studied here, only the line at 488 nm reaches the lasing threshold, since its gain is much higher than for the other potentially lasing lines in the Ar^+ discharge. Thus, an intracavity prism is not required for spectral line selection. A temperature-tuned intracavity étalon selects a single longitudinal mode. The laser cavity is approximately 96 cm long, giving a mode spacing of 156 MHz; our results indicate that the passive laser cavity has a finesse of 56.3, and hence a passive mode width $\Gamma_0/2\pi$ of 2.77 MHz full width at half maximum (FWHM) corresponding to a value of $\gamma_c\,(=\Gamma_0/2)$

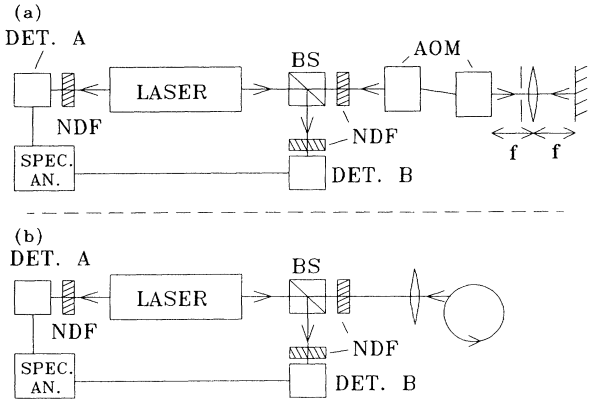

FIG. 8. The experimental arrangement. The upper diagram (a) depicts the system used in our Ar^+-laser study, in which a controllable detuned input is obtained by shifting the laser output with acousto-optic modulators (AOM) and reinjecting back into the laser cavity. NDF denotes a neutral density filter, BS a beamsplitter, and SPEC. AN. a spectrum analyzer. In the lower diagram (b), a Doppler-shifted input is generated by scattering the laser beam from a rotating wheel. In each case, detectors *A* and *B* are used independently to measure the transmission and reflection gain, respectively.

of 8.7×10^6 s^{-1}. The upper-state population decay rate $\gamma_\parallel$ has a value of approximately 4×10^8 s^{-1} [2], and the atomic dipole decay rate $\gamma_\perp$, which is found from the linewidth of the lasing transition, is $>10^{10}$ s^{-1} [39]. Rapid thermal motion of the excited ions ensures that spatial inhomogeneities of the gain medium (i.e., hole-burning effects) are insignificant at our moderate power levels. Thus, these rapid relaxation rates should ensure that the Ar^+ laser is an excellent approximation to class A (Sec. I). The laser output power can be varied over two orders of magnitude by adjustment of the discharge current: our quoted powers represent the output from one end only, that nearest the beamsplitter in Fig. 8(a).

The detuned signal for injection into the laser cavity is derived from the output of the laser itself. This is achieved by routing one of the output beams through two acousto-optic modulators (AOM's), which produce, respectively, a fixed shift of -80 MHz and a variable shift of $(80+\omega/4\pi)$ MHz in the beam frequency, where $\omega/4\pi$ can be varied over the range 0 to ±5 MHz. The beam then passes again through the modulators after reflection from the mirror, thus acquiring a frequency shift of $\omega/2\pi$ before it reenters the laser. The lens between the second AOM and the mirror ensures that the reflected beam always retraces its path back into the laser, independent of the frequency shift. The returning beam is attenuated by a factor of at least 10^5 to satisfy the small-signal requirements for linear amplification. The experiment thus becomes equivalent to one where the signal is produced by an independent source, but with the problems associated with frequency jitter significantly reduced. This is because any fluctuations in laser frequency caused by vibration-induced changes in cavity length are identical for both signal and amplifier, provided they occur on a time scale much slower than the round-trip time from the laser to the mirror and back ($\sim10^{-8}$ s). Above-threshold amplification of the return beam is examined both in transmission (detector A) and reflection (detector B). The incident power on the detector is limited with neutral density filters to <2 mW to avoid saturation. Each detector (Analog Modules type 713A) is exposed to the strong laser field at angular frequency ω_L, serving as a local oscillator, plus the weak transmitted or reflected beam, as modified by the above-threshold amplifier. The spectral response of the detectors and the optical efficiency of the modulators are uniform to better than 5% over the range 0–10 MHz.

The gain of the above-threshold amplifier is defined as the ratio of the *measured* beat signal power to that derived for the same input signal mixed, *before* reentering the laser, with an identical strength local oscillator. This corresponds to a determination of G_T [Eq. (5.31)] in transmission, and G_R [Eq. (5.34)] in reflection. The gains G_T and G_R were measured as functions of detuning $\omega/2\pi$ by spectral analysis of the detector output at a number of different values of laser power. The spectrum of this output consists of a single dominant peak at the detuning frequency, whose width is determined by the instrumental function of the analyzer, which always has a bandwidth <30 kHz. The gain is assumed to be unity at large detuning for the reflected beam [Eq. (5.34)], and the corresponding signal strength allows accurate calibration of absolute gains.

An alternative method for generation of a detuned input signal is to scatter the laser radiation from a moving target, such as a belt sander, or rotating ground glass disk [Fig. 8(b)]. This is a common technique in laser radar studies [40], and it was used here in preliminary investigations of the Ar^+ laser and also for examination of CO_2-laser gain behavior, as suitable acousto-optic modulators were not available at the 10-μm wavelength. A disadvantage of this technique is the spectral spread of the Doppler-shifted signal return, associated with the light's thermal character [40]. This bandwidth is usually frequency-shift dependent, and careful analysis must take this into account in order to determine the true gain profile. A further problem arises from the reproducibility of signal strength; this is very sensitive to beam focusing at the target.

Measurements of the Ar^+ intensity-fluctuation noise spectra are made by illuminating the detector with the laser output, suitably attenuated to avoid saturation. The current from the detector is then spectrum analyzed and averaged: the experiment thus requires only the equipment to the left of the laser in Fig. 8. The noise spectra are Lorentzian shapes, superimposed on a constant shot-noise background. The measurements of noise are considerably less accurate than for the gain. There are two reasons for this: because of the low level of the amplitude fluctuations the noise is inherently weak in comparison to shot noise, and any reduction of the effective quantum efficiency of the measurement, by attenuation, further reduces the sensitivity. In addition, the effect of acoustic vibrations and electrical disturbance causes an extra contribution to the low-frequency noise. This so-called "technical" noise typically lies within about 200 kHz, and it distorts the profiles from the pure Lorentzian noise spectra predicted by theory. Examples of technical noise might arise from any residual 50-Hz mains ripple, or from optical-table resonances excited by turbulence from the laser-cooling water. The noise bandwidth measurements here therefore have uncertainties of at least 10%, increasing at the higher levels of laser power.

A. The Ar^+ laser (class A)

Figure 9 shows some typical gain profiles for the heterodyne beat signal in transmission. The profiles are well-behaved Lorentzian functions whose widths and peak gains are strong functions of laser power. This is in qualitative accord with the predictions of (5.31); there is further agreement in the invariance of the square root of the peak gain-bandwidth product.

In Fig. 6 we showed a plot of experimental values of peak gain and bandwidth of both gain *and* noise as functions of the laser pumping rate C. Also plotted are the theoretical predictions both below [(4.7) and (4.9)] and above [(5.18) and (5.32)] threshold for the symmetric cavity case ($\gamma_1=\gamma_2$). The values of cavity loss rate γ_c and saturation power P_S, which relates laser power P to pumping rate C (3.10), have been chosen to optimize the agreement between experiment and theory: Fig. 6 shows

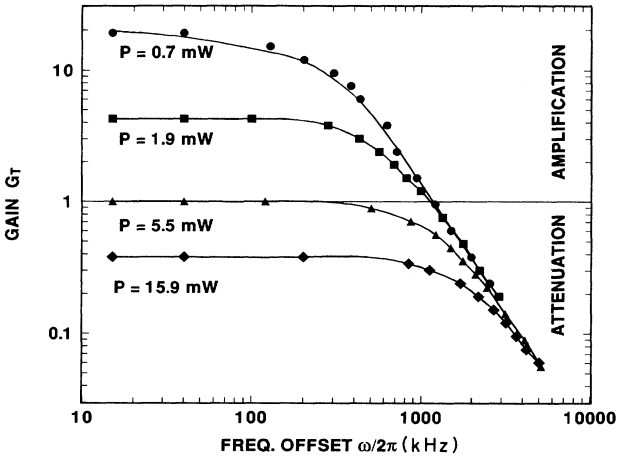

FIG. 9. Experimental profiles for heterodyne gain in transmission G_T at different Ar^+-laser powers. The Lorentzian shape, characteristic of class-A lasers, is clearly evident.

this to be excellent. The optimum value of γ_c (8.7×10^6 s^{-1}) is consistent with estimates based on the mirror reflectivities and cavity length.

Good agreement between theory and experiment is also obtained for the gain in reflection (Fig. 7). The profiles have the form shown in Fig. 7 of $1 \pm$ (a Lorentzian function) [Eq. (5.34)]. A quantitative check was made of the particularly notable features of Fig. 7: the flat frequency response occurs at an output power $P=1.67$ mW ($C=1.3$) and zero gain for $\omega\rightarrow0$ is achieved at a three-times-greater power of $P=4.92$ mW ($C=1.9$).

B. The CO_2 laser (class B)

Figure 10 shows a gain profile obtained with an Edinburgh Instruments Model CM1000 CO_2 waveguide laser, running at a wavelength of 10.6 μm. The laser pumping rate is not adjustable, and hence a systematic study cannot be carried out as in the case of Ar^+; however, the behavior in Fig. 10 demonstrates the features predicted for class-B lasers by the general gain expression (5.17). The double-peaked character is immediately apparent. The increased gain at a detuning of $\omega/2\pi=\pm0.6$ MHz may be interpreted as a resonant enhancement of the natural laser relaxation oscillations as discussed in Sec. V A. Relaxation of the upper-state population in CO_2 is dominated by collisional deexcitation [41], with $\gamma_\parallel$ ranging from 10^5 to 10^7 s^{-1}, depending on the gas pressure. Attempts to fit the theoretical expression for the gain (5.17) to the data with reasonable parameter values ($\gamma_\parallel=10^5$ s^{-1}, $\gamma_c=10^7$ s^{-1}, $C=4$) were unsuccessful (dashed curve of Fig. 10). However, when the possibility of a lower-level population is included, an acceptable fit can be obtained. The solid curve shows the prediction of Eq. (A16) from the Appendix, with $\gamma_l=3\times10^6$ s^{-1}. This demonstrates the sensitivity of the gain curves to buildup of population in the lower lasing level for the class-B laser.

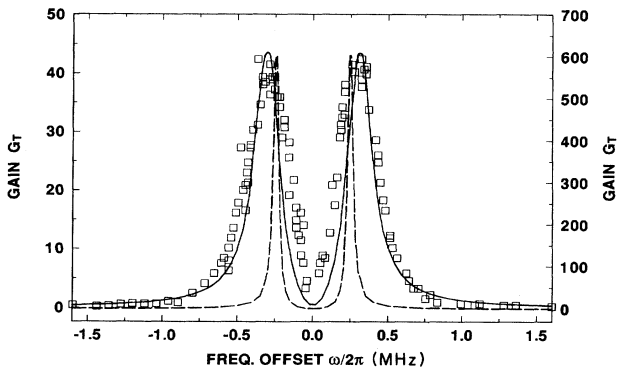

FIG. 10. Heterodyne gain profile for a CO_2 laser (class B). The double-peaked shape is closely related to the phenomenon of relaxation oscillations. The dashed curve (right-hand scale) is a theoretical prediction ignoring lower-level population. The solid curve (left-hand scale) takes this population into account. □, data points (left-hand scale).

Preliminary experiments with a custom-built CO_2 laser system [42] in which the pressure can be adjusted to change the value of $\gamma_\parallel$ indicate that the gain peaks do indeed move to higher frequency at larger $\gamma_\parallel$. The peaks also behave similarly as the pumping rate C is increased.

VII. CONCLUSIONS

We have presented a unified comprehensive theory for the gain, noise, and signal-to-noise ratio of a class-A or class-B laser operated below or above its oscillation threshold. We have also reported measurements, particularly of the gain characteristics, for both classes of laser above threshold. The theory and the measurements are in excellent agreement.

The properties of a laser amplifier below threshold are quite well known, and the output light of the free-running device is purely chaotic noise with a Lorentzian spectrum whose bandwidth diminishes as threshold is approached. We have also calculated the corresponding gain profile for linear amplification of an injected signal and have shown that it is properly related to the noise spectrum in the manner demanded by the general theory of phase-insensitive linear amplifiers [21]. The resulting signal-to-noise ratio of the laser amplifier below threshold is such that its use can provide significant enhancement in the sensitivity of heterodyne detection when photodetectors of low efficiency are used, but the improvement is negligible for high-efficiency photodetectors.

Above the oscillation threshold, we have shown that the physics of the laser amplification process is considerably more complex. Pulsations in the population inversion lead to four-wave mixing and the correlation of signal and image components in both the gain and the noise. These correlations often tend to reduce the gain and the noise that would occur for observations of the signal or image frequencies alone, particularly at small detunings from the laser frequency. Twin-beam noise correlations are of course well known; they occur in both four-wave mixing [18] and in parametric oscillation or down-conversion [43], where the noise correlations have been used to generate light with sub-Poissonian photon statis-

tics. We believe, however, that the important effects of correlations between signal and image frequencies in determining the gain profile and noise spectrum of the ordinary gas laser have not previously been emphasized.

The gain profile of the laser has apparently been neither calculated nor measured before. For class-A lasers, where the gain profile has a Lorentzian peak centered on the laser frequency, gains greater than unity occur only for values of the cooperation parameter C that lie between 1 and 2. Our calculations of the gain profile have been supported by detailed measurements on an argon-ion laser, which confirm the expected increase in gain bandwidth and decrease in peak gain with increasing laser power or cooperation parameter C. For class-B lasers, where the gain profile generally has two peaks symmetrically placed on either side of the laser frequency, gains greater than unity persist in the regions of the peaks for values of C larger than 2. The occurrence of a double-peaked gain profile for class-B lasers has been confirmed by measurements on a CO_2 laser.

The calculation of the noise spectrum of the laser above threshold given here parallels previous work [7,10,35]. The spectrum has a single Lorentzian peak for class-A lasers and it generally has a double-peaked form for class-B lasers, in accordance with the required intimate relationship between gain and noise. A similar double-peaked noise spectrum occurs for semiconductor lasers, where a more complicated theory is needed to take account of additional phase fluctuations that are driven by modulation of the refractive index by carrier density fluctuations [6]. For the class-A laser, we have shown that, as expected on general grounds [21], the use of an above-threshold laser preamplifier in direct detection leads to a factor-of-2 degradation in signal-to-noise ratio when perfectly efficient ($\eta=1$) photodetectors are used. However, amplification can again lead to significant enhancements in signal-to-noise ratio when the photodetector efficiency is sufficiently low.

A noteworthy feature of the laser oscillation threshold is its close analogy to a second-order thermodynamic phase transition [12]. The gain profiles calculated and measured here show all of the properties expected of the linear susceptibilities associated with a phase transition, in terms of bandwidths that tend to zero and peak magnitudes that tend to infinity as the threshold is approached from above or below. The noise spectrum of the laser emission also shows characteristic properties in the threshold region, which are summarized as follows. The laser emission below threshold consists entirely of chaotic noise whose bandwidth

$$\Gamma=2\gamma_c(1-C)=2\gamma_c C/\langle n\rangle \tag{7.1}$$

from (4.27) and (4.28) is identical to that of the gain profile. Above threshold, it is possible to identify two distinct components in the emission spectrum [20]. The first coherent component accounts for almost all of the mean number $|\alpha_L|^2$ of photons excited in the cavity, and its bandwidth

$$\Gamma_L=\gamma_c/|\alpha_L|^2 , \tag{7.2}$$

given by (5.60), is controlled by phase diffusion. This bandwidth shows a factor-of-2 reduction at threshold ($C=1$) in comparison to the below-threshold result when these are expressed in terms of the mean photon number, as in the second form of (7.1). The second noise component, of mean intracavity photon number $1/4(C-1)$, results from the residual amplitude fluctuations above threshold, and its bandwidth

$$\Gamma_N=4\gamma_c(C-1)/C \tag{7.3}$$

from (5.62) is identical to that of the gain profile. In comparison with the below-threshold result given in the first form of (7.1), this bandwidth is increased by a factor of 2 and C is replaced by $1/C$.

Further consideration needs to be given to the bandwidths that are determined by measurements of the intensity-fluctuation spectra of the laser emission. Thus below threshold the intensity fluctuations result from the beating of the emitted chaotic noise with itself, and the bandwidth obtained from (7.1) is

$$2\Gamma=4\gamma_c(1-C) . \tag{7.4}$$

Above threshold, the phase diffusion plays no role in intensity measurements and the main contribution results from the beating of the very strong coherent laser component with the very weak amplitude-fluctuation noise component, to give a bandwidth that is unchanged from (7.3). Thus, in comparing the above-threshold bandwidth with its below-threshold form (7.4), C is again replaced by $1/C$ but there is no additional factor of 2 [30].

All of the above discussion refers to determinations of the gain and the noise in which signal and image frequencies are detected with equal efficiencies. It is possible in principle to remove the signal or image frequencies by filtering. We have shown that, although such filtering can produce large increases in the gain, there are also correspondingly large increases in the noise, to the extent that no improvement in signal-to-noise ratio is possible. We have not been able to back up our calculations of these effects by measurements, since it is not feasible to filter out one side of the relatively narrow argon-ion laser line. However, we have made gain and noise measurements on the subthreshold cavity modes on either side of the laser mode [2,3]. These show very similar four-wave-mixing correlations to those considered here for frequencies within the laser mode itself, and the relatively large spacing of the adjacent modes makes it straightforward to filter out the signal or image frequency components. The theory and experiments for the adjacent modes will be presented separately [38].

Finally, our study of the gain and noise of the above-threshold laser clarifies the physical processes that underlie the operation of so-called "autodyne" lidar systems. Such lidars have been in existence for over 20 years [22]; this work represents a comprehensive study of their behavior. The results presented in Sec. V may be used to assess the optimum conditions under which to run an autodyne system. The laser parameters chosen to optimize performance will depend upon the precise application. Of particular importance are considerations such as signal bandwidth, photodetector sensitivity, and maximum

detector incident power level. Thus, the expressions in Sec. V demonstrate that bandwidth, gain, output power, and SNR are all sensitive to adjustments in pumping rate C, total cavity loss rate γ_c, front-to-back mirror asymmetry ratio γ_2/γ_1, as well as the population inversion relaxation parameter $\gamma_\parallel$. A detailed analysis of autodyne behavior and optimization will be presented later [44].

ACKNOWLEDGMENTS

We acknowledge useful discussions with Dr. C. Hill and Dr. E. Jakeman of the Defence Research Agency, Malvern, UK and with Dr. G. L. Mander of the Amarvati Buddhist Monastery, Hemel Hempstead, UK. M. H. is funded by a Ministry of Defence research agreement with the University of Essex.

APPENDIX: NONZERO LOWER-LEVEL POPULATION

The calculations in the paper are all based on a model in which the population of the lower level of the laser transition is assumed to be negligible. In this appendix we summarize the results that are obtained when the laser model is generalized to allow a nonzero lower-level population.

Let the populations of the upper and lower laser levels be denoted U and L, respectively, so that the population inversion is

$$D=U-L \ . \tag{A1}$$

Suppose that the two levels are pumped at rates R_u and R_l, respectively, and that the decay rate of the lower-level population is γ_l. The equations of motion (2.6) and (2.8) for the cavity field and atomic dipole moment remain the same in the more general model, but the equation of motion (2.7) for the population inversion is replaced by equations for the individual laser levels,

$$\dot{U}+\gamma_\parallel U=R_u-g(\alpha^* d+\alpha d^*)+\Gamma_u \ , \tag{A2}$$

$$\dot{L}+\gamma_l L=R_l+\gamma_\parallel U+g(\alpha^* d+\alpha d^*)+\Gamma_l \ , \tag{A3}$$

where Γ_u and Γ_l are Langevin forces for the two levels. With class-C lasers again excluded from consideration, the atomic dipole equation of motion reduces to (2.15).

1. Free-running laser

The calculation generalizes that given in Sec. III. Thus (3.4) applies below threshold, where the level populations are

$$U_0=R_u/\gamma_\parallel \equiv U_p \tag{A4}$$

and

$$L_0=(R_l+R_u)/\gamma_l \equiv L_p \ . \tag{A5}$$

The model parameters are assumed to have values that ensure the inequality $U_p>L_p$, and the population inversion is

$$D_0=U_0-L_0=U_p-L_p \equiv D_p \ . \tag{A6}$$

The cooperation parameter C is still defined by (3.5).

The expressions (3.6)–(3.9) remain valid for the laser above threshold, where the upper-level population is now

$$U_0=\frac{R_l+R_u}{\gamma_l}+\frac{\gamma_c\gamma_\perp}{g^2} \tag{A7}$$

and the lower-level population is again given by (A5). It is readily verified that the upper-level populations given by (A4) below threshold and (A7) above threshold are equal at $C=1$.

The population equations of motion (A2) and (A3) are conveniently rewritten in terms of the population inversion D defined in (A1) instead of the upper-level population U. With the pumping rates also expressed in terms of the populations D_p and L_p obtained in the absence of laser action, (A2) and (A3) give

$$\dot{D}=2\gamma_\parallel(D_p-D)-(\gamma_l-2\gamma_\parallel)(L_p-L) -2g(\alpha^* d+\alpha d^*)+\Gamma_u-\Gamma_l \tag{A8}$$

and

$$\dot{L}=-\gamma_\parallel(D_p-D)+(\gamma_l-\gamma_\parallel)(L_p-L) +g(\alpha^* d+\alpha d^*)+\Gamma_l \ . \tag{A9}$$

The forms of solution of the equations of motion (2.6), (2.15), (A8), and (A9) are as given in (2.11)–(2.13), with a mean lower-level population given by

$$L=L_0+L_1\exp(-i\omega t)+L_1^*\exp(i\omega t) \ . \tag{A10}$$

2. Below-threshold gain

The calculation parallels that given in Sec. IV A, with L_1 set equal to zero, in addition to the conditions imposed in (4.1). It is easily shown that the gain is unaffected by the presence of a nonzero lower-level population, and, for example, the expression (4.6) for the intensity gain in transmission remains valid.

3. Below-threshold noise

The calculation parallels that given in Sec. IV B with zero-mean fluctuations in the field and the population inversion represented by (4.13) and (4.14), respectively, and fluctuations in the lower-level population represented by

$$L(t)=L_p+\delta L(t) \ . \tag{A11}$$

As far as the fluctuations in cavity field are concerned, the equation of motion (4.15) is unchanged, and their power spectrum is still given by (4.20). However, the result given by Louisell [10] for the required Langevin force correlation function is modified by the presence of a nonzero mean lower-level population so that (4.22) is replaced by

$$\langle \Gamma_d^*(\omega_L+\omega)\Gamma_d(\omega_L+\omega')\rangle=2\gamma_\perp(D_0+L_0)\delta(\omega-\omega') \ . \tag{A12}$$

The cavity-field noise power spectrum (4.24) is accordingly multiplied by an additional population factor

$$\mathcal{P}=1+\frac{L_0}{D_0}=\frac{U_0}{U_0-L_0}\ , \tag{A13}$$

whose occurrence in the noise output of inverted population amplifiers is well known (see, for example, [25]). The same factor occurs in the mean photon number $\langle n\rangle$ given by (4.27), and, for example, the intensity noise spectrum (4.43) is correspondingly modified.

4. Above-threshold gain

The method of calculation follows that of Sec. V A. Thus (5.1) and (5.2) remain valid, but (5.3) is replaced by the pair of equations obtained from (A8) and (A9)

$$(2\gamma_\parallel-i\omega)D_1=(\gamma_l-2\gamma_\parallel)L_1 -(4g^2/\gamma_\perp)[|\alpha_L|^2D_1+(\alpha_L^*\alpha_S+\alpha_L\alpha_I^*)D_0] \tag{A14}$$

and

$$(\gamma_l-\gamma_\parallel-i\omega)L_1 =\gamma_\parallel D_1+(2g^2/\gamma_\perp)[|\alpha_L|^2D_1+(\alpha_L^*\alpha_S+\alpha_L\alpha_I^*)D_0]\ . \tag{A15}$$

There are four equations for the four unknowns α_S, α_I^*, D_1, and L_1, and these can be solved without difficulty. The resulting expression for the transmission gain defined in accordance with (5.15) and (5.17) is

$$G_T(\omega)=\gamma_1\gamma_2\{\omega^2[\gamma_l+\gamma_\parallel(2C-1)]^2 +(\gamma_l\gamma_\parallel C-\omega^2)^2\}/\mathcal{D}_{\text{den}'}\ , \tag{A16}$$

where

$$\mathcal{D}_{\text{den}'}=\omega^2[\gamma_l\gamma_\parallel C+4\gamma_\parallel\gamma_c(C-1)-\omega^2]^2 +[\gamma_l\omega^2-2\gamma_l\gamma_\parallel\gamma_c(C-1) +\omega^2\gamma_\parallel(2C-1)]^2\ . \tag{A17}$$

This result correctly reduces to the transmission gain derived in (5.17) when the lower-level population is made negligible by taking γ_l to be much larger than the other decay rates. For the class-A laser ($\gamma_\parallel$, $\gamma_l\gg\gamma_c$), the gain G_T is unaffected by any lower-level population. In this case, Eq. (A17) reduces to the earlier expression (5.31). However, for the class-B laser, the presence of a lower-level population leads to broadening of the relaxation oscillation peaks as well as their shift to higher frequency. It is likely that this will be an important factor in determining the CO_2-laser gain profile.

5. Above-threshold noise

The calculation parallels that given in Sec. V B with the fluctuations in field and population inversion represented by (5.37) and (5.38), respectively, and fluctuations in the lower-level population represented by

$$L(t)=L_0+\delta L(t)\ . \tag{A18}$$

The equation of motion (5.39) for the field fluctuation is unchanged but (5.40) is replaced by the pair of equations

$$\delta\dot{D}(t)+2\gamma_\parallel C\delta D(t)-(\gamma_l-2\gamma_\parallel)\delta L(t)+8\gamma_c|\alpha_L|\delta\alpha(t) =-(2g|\alpha_L|/\gamma_\perp)\{\Gamma_d(t)\exp[-i\delta\phi(t)+i\omega_L t]+\text{c.c.}\}+\Gamma_u(t)-\Gamma_l(t) \tag{A19}$$

and

$$\delta\dot{L}(t)+(\gamma_l-\gamma_\parallel)\delta L(t)-\gamma_\parallel C\delta D(t)-4\gamma_c|\alpha_L|\delta\alpha(t)=(g|\alpha_L|/\gamma_\perp)\{\Gamma_d(t)\exp[-i\delta\phi(t)+i\omega_L t]+\text{c.c.}\}+\Gamma_l(t)\ . \tag{A20}$$

The real and imaginary parts of (5.39) are separated as before, and the calculation of the phase fluctuation power spectrum is unchanged except that the Langevin force correlation function (5.47) is replaced by (A12). The phase diffusion linewidth is accordingly given by the Schawlow-Townes expression (5.60) multiplied by the population factor $\mathcal{P}$ from (A13). This effect of a nonzero lower-level atomic population is well known [11,20,33].

The calculation of the corresponding amplitude fluctuation power spectrum is more difficult, since it entails simultaneous solution of the real parts of (5.39), (A19), and (A20). It is found after some algebra that (5.49) is replaced by

$$\langle\delta\alpha(\omega)\delta\alpha(\omega')\rangle=\gamma_c\{\mathcal{P}[\omega^4+\omega^2\gamma_l^2+\omega^2\gamma_\parallel^2(2C-1)+\omega^2\gamma_l\gamma_\parallel(C-1)+\gamma_l^2\gamma_\parallel^2C] -\omega^2\gamma_l\gamma_\parallel(C-1)-2\omega^2\gamma_\parallel^2(C-1)^2-\gamma_l\gamma_\parallel^3C(C-1)\}\delta(\omega+\omega')/\mathcal{D}_{\text{den}'}\ . \tag{A21}$$

This result correctly reduces to (5.49) when $\mathcal{P}$ is set equal to unity and γ_l is much larger than the other decay rates. The class-A laser limit is obtained as $\gamma_\parallel\to\infty$. However, as $\gamma_l>\gamma_\parallel$, we must also allow $\gamma_l\to\infty$, but require that $L_0=(R_l+R_u)/\gamma_l$ remain finite.

[1] M. Harris, R. Loudon, G. L. Mander, and J. M. Vaughan, Phys. Rev. Lett. **67**, 1743 (1991).

[2] M. Harris, R. Loudon, T. J. Shepherd, and J. M. Vaughan, Opt. Commun. **91**, 383 (1992).

[3] M. Harris, R. Loudon, T. J. Shepherd, and J. M. Vaughan, Phys. Rev. Lett. **69**, 2360 (1992).

[4] M. O. Scully and W. E. Lamb, Phys. Rev. **159**, 208 (1967).

[5] M. Sargent, M. O. Scully, and W. E. Lamb, *Laser Physics*

(Addison-Wesley, Reading, MA, 1974).
[6] C. H. Henry, IEEE J. Quantum Electron. **QE-18**, 259 (1982); K. Vahala, C. Harder, and A. Yariv, Appl. Phys. Lett. **42**, 211 (1983); M. P. van Exter, W. A. Hamel, J. P. Woerdman, and B. R. P. Zeilemans, IEEE J. Quantum Electron. **28**, 1470 (1992).
[7] Y. Yamamoto and N. Imoto, IEEE J. Quantum Electron. **QE-22**, 2032 (1986).
[8] R. G. Harrison and D. J. Biswas, Prog. Quantum Electron. **10**, 147 (1985).
[9] M. J. Collett and C. W. Gardiner, Phys. Rev. A **30**, 1386 (1984).
[10] W. H. Louisell, *Quantum Statistical Properties of Radiation* (Wiley, New York, 1973).
[11] A. E. Siegman, *Lasers* (University Science Books, Mill Valley, CA, 1986).
[12] V. DeGiorgio and M. O. Scully, Phys. Rev. A **2**, 1170 (1970).
[13] R. H. Pantell, Proc. IEEE **53**, 474 (1965).
[14] M. B. Spencer and W. E. Lamb, Phys. Rev. A **5**, 884 (1972).
[15] H. Haken, *Light Vol. 2: Laser Light Dynamics* (North-Holland, Amsterdam, 1985).
[16] D. K. Bandy, L. A. Lugiato, and L. M. Narducci, in *Instabilities and Chaos in Quantum Optics,* edited by F. T. Arecchi and R. G. Harrison (Springer-Verlag, Berlin, 1987); D. J. Jones and D. K. Bandy, J. Opt. Soc. Am. B **7**, 2119 (1990); J. Mørk, J. Mark, and B. Tromborg, Phys. Rev. Lett. **65**, 1999 (1990).
[17] R. Frey, Opt. Lett. **11**, 91 (1986).
[18] M. D. Reid and D. F. Walls, Phys. Rev. A **34**, 4929 (1986); W. Zhang and D. F. Walls, *ibid.* **41**, 6385 (1990); M. Brambilla, F. Castelli, L. A. Lugiato, F. Prati, and G. Strini, Opt. Commun. **83**, 367 (1991).
[19] G. P. Agrawal, J. Opt. Soc. Am. B **5**, 147 (1988); M. Yamada, J. Appl. Phys. **66**, 81 (1989); F. L. Zhou, M. Sargent, S. W. Koch, and W. W. Chow, Phys. Rev. A **41**, 463 (1990).
[20] H. Haken, *Laser Theory* (Springer-Verlag, Berlin, 1984).
[21] C. M. Caves, Phys. Rev. D **26**, 1817 (1982).
[22] M. J. Rudd, J. Phys. E **1**, 723 (1968); R. F. Kazarinov and R. A. Suris, Zh. Eksp. Teor. Fiz. **65**, 2137 (1973) [Sov. Phys. JETP **66**, 1067 (1974)]; J. H. Churnside, Appl. Opt. **23**, 61 (1984); A. P. Godlevskii, E. P. Gordov, Y. Y. Ponurovskii, A. Z. Fazliev, and P. P. Sharin, *ibid.* **26**, 1607 (1987); P. J. de Groot and G. M. Gallatin, Opt. Lett. **14**, 165 (1989).
[23] The term "autodyne" has also been used previously to describe a rather different effect, that of self-beating light spectroscopy. See, for example, D. U. Fluckiger, R. J. Keyes, and J. H. Shapiro, Appl. Opt. **26**, 318 (1987).
[24] The derivation and background to the laser equations appears in several standard texts. See, for example, Ref. [11], Chap. 24; the basic laser equations are given in (24.56). See also Ref. [5], Chap. 8 and Ref. [10], Chap. 9.
[25] G. L. Mander, R. Loudon, and T. J. Shepherd, Phys. Rev. A **40**, 5753 (1989).
[26] R. Loudon, *The Quantum Theory of Light,* 2nd ed. (Clarendon, Oxford, 1983).
[27] K. J. Blow, R. Loudon, S. J. D. Phoenix, and T. J. Shepherd, Phys. Rev. A **42**, 4102 (1990).
[28] M. Harris, R. Loudon, T. J. Shepherd, and J. M. Vaughan, J. Mod. Opt. **39**, 1195 (1992).
[29] R. Hanbury Brown, *The Intensity Interferometer* (Taylor and Francis, London, 1974).
[30] E. Jakeman and R. Loudon, J. Phys. A **24**, 5339 (1991).
[31] R. Loudon, in *Order and Chaos in Nonlinear Physical Systems,* edited by S. Lundqvist *et al.* (Plenum, New York, 1988), p. 225.
[32] H. Risken, Z. Phys. **186**, 85 (1965).
[33] A. L. Schawlow and C. H. Townes, Phys. Rev. **112**, 1940 (1958).
[34] H. Gerhardt, H. Welling, and A. Güttner, Phys. Lett. **40A**, 191 (1972).
[35] M. Lax, IEEE J. Quantum Electron. **QE-3**, 37 (1967).
[36] D. E. McCumber, Phys. Rev. **141**, 306 (1966).
[37] R. Centeno Neelen, D. M. Boersma, M. P. van Exter, C. Nienhuis, and J. P. Woerdman, Phys. Rev. Lett. **69**, 593 (1992).
[38] R. Loudon, M. Harris, T. J. Shepherd, and J. M. Vaughan (unpublished).
[39] M. Harris, R. Loudon, T. J. Shepherd, and J. M. Vaughan, J. Mod. Opt. **38**, 613 (1991).
[40] J. M. Vaughan, D. Brown, R. D. Callan, P. H. Davies, R. Foord, and W. R. M. Pomeroy, J. Mod. Opt. **38**, 623 (1991).
[41] A. Yariv, *Quantum Electronics,* 3rd ed. (Wiley, New York, 1989).
[42] C. A. Hill and J. W. H. Perry (private communication).
[43] P. R. Tapster, J. G. Rarity, and J. S. Satchell, Phys. Rev. A **37**, 2963 (1988); J. Mertz, A. Heidmann, C. Fabre, E. Giacobino, and S. Reynaud, Phys. Rev. Lett. **64**, 2897 (1990); J. Mertz, A. Heidmann, and C. Fabre, Phys. Rev. A **44**, 3229 (1991); C. Kim and P. Kumar, *ibid.* **45**, 5237 (1992).
[44] J. M. Vaughan, T. J. Shepherd, M. Harris, and R. Loudon (unpublished).